

Chapter 5

American Superconductor: Second Generation Superconductor Wire—From Research to Power Grid Applications

Srivatsan Sathyamurthy, Cees Thieme and Martin W. Rupich

Abstract American Superconductor Corporation (AMSC) is the leader the development, manufacturing and deployment of high temperature superconducting (HTS) wire. The company's HTS wire, called Amperium HTS wire, is the result of decades of a research and development effort on texturing of metals, epitaxial growth of complex oxides and innovative roll-to-roll manufacturing techniques. AMSC is also a leader in developing HTS wire based products that are being deployed in the power grid around the world. In this chapter we provide an overview of the high temperature superconducting materials, describe the challenges overcome in converting these materials into useful wires and summarize the major markets for the Amperium wire.

5.1 Introduction

American Superconductor Corporation (AMSC) was established in 1987, shortly after the discovery of the cuprate based high temperature superconductors, with the goal of developing these newly discovered materials for use in commercial applications. Since its founding, AMSC has been a world leader in the development and manufacturing of HTS (high temperature superconducting) wire for a broad range of commercial and military applications. While AMSC focused on the development of HTS wire, it evolved into a broad-based energy company that supplies innovative products and services to the both the wind and power grid markets. AMSC's focus is now on providing the world with cleaner, greener and more secure energy solutions based on both conventional and innovative HTS-based technologies. AMSC's HTS wire remains a core company technology and as it matures, it is being incorporated into a growing range of products providing innovative solutions to increase the power grid's capacity, reliability, security and efficiency.

S. Sathyamurthy (✉) · C. Thieme · M.W. Rupich
Materials R&D, AMSC, 64 Jackson Road, Devens, MA 01434, USA
e-mail: Srivatsan.Sathyamurthy@amsc.com

5.1.1 Cuprate-Based High Temperature Superconductors

Over a quarter of a century after the discovery of the cuprate based $(\text{RE})\text{Ba}_2\text{Cu}_3\text{O}_{7-x}$ ($(\text{RE})\text{BCO}$ where $\text{RE} = \text{rare earth}$) HTS materials with superconducting transition temperatures (T_c) above liquid nitrogen temperature (77 K), the first commercial applications of HTS wires are beginning to be realized. Although their discovery in 1987 was accompanied by vast excitement and visions of near-term applications, it was soon realized that the materials were complex oxides that would require a formidable research and development effort to understand and transform them into usable conductors for real-world applications. Today, after extensive development effort, American Superconductor Corporation (AMSC) and a number of other manufacturers are producing the HTS wire, typically referred to as 2G or second generation HTS wire, in continuous lengths with the performance level required for these initial commercial applications, as shown in Fig. 5.1. (First generation or 1G HTS wire is based on the BiSrCaCuO -based materials described below [1].) These wires are now being used in fault current limiters (FCL's) that are being deployed in the electrical grid and in a number of cable projects around the world [2–5]. The first 2G HTS wire-based cable installed in an actual electrical grid, a 500 m long DC cable produced by Cable Systems and the Korean Electric Power Company (KEPCO) using AMSC 2G HTS wire, was energized on Jeju Island, Korea in September 2014 [6]. This will be followed by longer cables projects currently being installed or planned in Korea and the United States.

Within months of the material discovery, the first $(\text{RE})\text{Ba}_2\text{Cu}_3\text{O}_{7-x}$ wire was initially fabricated by Jin at Bell Labs using an oxide-powder-in-tube (OPIT) approach [7]; however, it carried a critical current density, J_c , of only 175 A/cm^2 (77 K, self-field), orders of magnitude lower than required for practical conductors. Early studies of the $(\text{RE})\text{BCO}$ materials found the low critical current in polycrystalline samples, such as used in Jin's first wire, arose from the fundamental physics of the cuprate materials; specifically, a short coherence length and the correlated character of their electron systems made them extremely sensitive to the

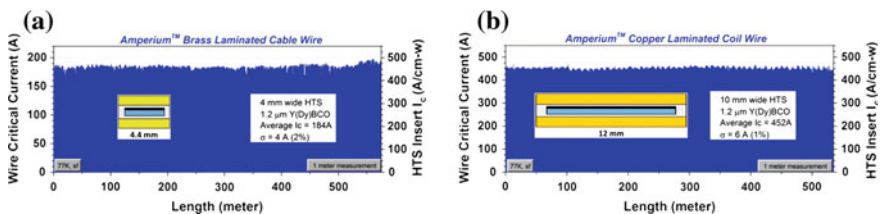


Fig. 5.1 Critical current as a function of length for 2G HTS wire manufactured by AMSC. The 2G HTS cable wire (a) is brass laminated with dimensions of $4.4 \text{ mm} \times 0.3 \text{ mm}$ and the 2G HTS coil wire (b) is copper laminated with dimensions of $12 \text{ mm} \times 0.4 \text{ mm}$ (courtesy of AMSC). Other manufacturers are also producing wire with comparable properties

grain boundary misorientations. Since epitaxial $\text{YBa}_2\text{Cu}_3\text{O}_{7-x}$ films had critical current densities of over 10^6 A/cm^2 at 77 K, it was thought that the manufacture of long length (RE)BCO based wires would require km-length single crystals, a challenge with no clear solution. Thus within 3 years of their discovery, reports began to appear stating that (RE)BCO was inherently incapable of carrying enough current to be useful and that development of (RE)BCO wire faced insurmountable obstacles [8, 9].

As a result, wire development efforts turned to the BiSrCaCuO-based materials (i.e., $\text{Bi(Pb)}_2\text{-Sr}_2\text{Ca}_2\text{Cu}_3\text{O}_x$) which could be uni-axially textured (*c*-axis grain alignment only) through thermo-mechanical processing using powder-in-tube methods [10]. Although there was no alignment of the *ab*-planes in the BSCCO materials, the wire, typically referred to as the first generation or 1G wire, carried significantly higher critical current due to a brick-wall type stacking of the platelet-shaped grains that produced a large effective grain boundary area that compensated for the weak linked grain boundaries [11, 12].

AMSC and Sumitomo Electric Industries (SEI) pursued this 1G technology and were instrumental in establishing the technical viability of HTS wires for various applications in the electrical power industry and rotating machinery by the mid 1990s [13]. Meanwhile, researchers around the world continued studying the (RE) $\text{Ba}_2\text{Cu}_3\text{O}_{7-x}$ materials, searching for innovative ways to overcome their fundamental limitations and routes around the seemingly insurmountable obstacles to practical long-length conductors.

5.2 (RE)BCO Structure and Properties

The (RE)BCO-based high temperature superconductors have a perovskite-type crystal structure, as shown in Fig. 5.2 (where RE = Y), in which two CuO_2 layers surround the RE atom separate CuO chains are oriented along the *b*-axis in another layer. Superconductivity occurs in the CuO_2 planes, while the CuO chains are

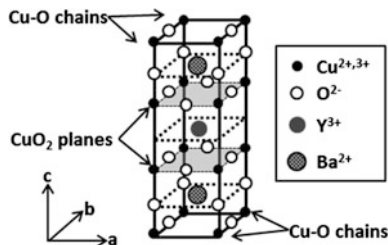


Fig. 5.2 Unit cell crystal structure of the (RE) $\text{Ba}_2\text{Cu}_3\text{O}_{7-x}$ cuprate superconductor. The RE atom is located between the two CuO_2 planes. Superconductivity is confined to the CuO_2 planes while the CuO chains, which are oriented along the *b*-axis serve as charge reservoirs providing carriers to the CuO_2 planes

principally charge reservoirs providing carriers to the CuO_2 planes depending on the oxygen content, expressed by $(7 - x)$ in the chemical formula of $(\text{RE})\text{Ba}_2\text{Cu}_3\text{O}_{7-x}$. A low oxygen content (large x), produces an electrically insulating tetragonal structure while a higher oxygen content ($x < 0.65$) converts the material into a superconducting orthorhombic structure, with a peak superconducting transition temperature (T_c) occurring at $x \sim 0.07$. This planar CuO_2 structure produces a large anisotropy in the superconducting properties of the $(\text{RE})\text{BCO}$ materials, resulting in the supercurrent in the a - b plane being much greater than along the c -axis [14, 15].

As mention earlier, the coherence length, (ξ), which can be described in simple terms as the spatial distance over which the paired superconducting electrons interact, is small in the $(\text{RE})\text{BCO}$ materials—1 to 4 nm in the ab -plane and less than 1 nm along the c -axis [16] (for comparison the ξ in pure elemental type-I superconductors is ~ 1000 nm and in the type II superconductors such as NbTi is ~ 5 nm). Consequently small disruptions in the lattice periodicity, such as high angle grain boundaries, appear as planar defects that drastically restrict the supercurrent flow from grain to grain.

A study of the effect of grain boundary misorientation on supercurrent flow, by Dimos, Chaudhari and Mannhart in 1990, found that the critical current density (J_c) across a grain boundary is nearly unaffected for grain boundary misorientations of less than 4° , but decreases exponentially for a misorientation angle greater than 4° [17, 18], as shown in the Fig. 5.3. In addition, they established that the J_c across grain boundaries was independent of the type (twist, tilt) of grain misorientation.

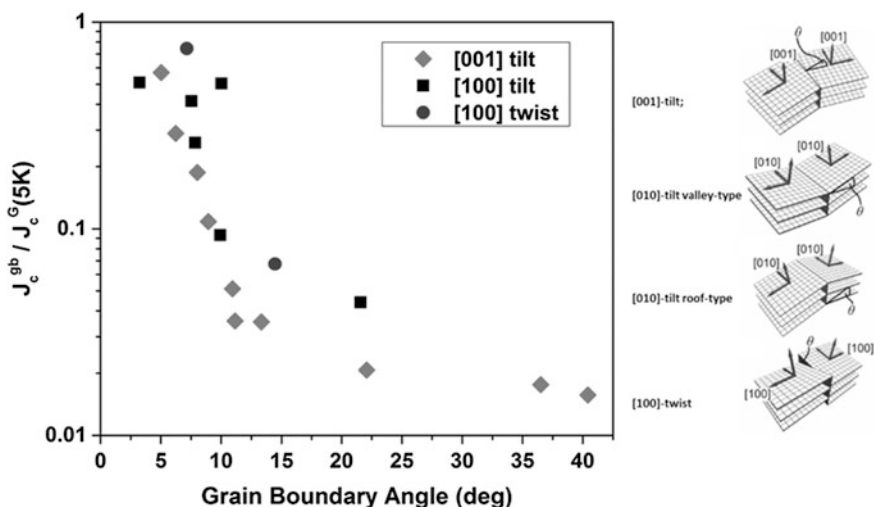


Fig. 5.3 The study by Dimos et al. [17] of YBCO films on bi-crystals showed the effect of **a** grain boundary misalignment and **b** grain boundary type, in the $(\text{RE})\text{BCO}$ materials and helped stimulate the development of textured templates for $(\text{RE})\text{BCO}$ coated conductors

These fundamental properties indicated that in order to carry high critical currents, the (RE)BCO materials would need to be textured with very clean grain boundaries and for fabricating practical conductors, this would need to be accomplished over lengths of 100s–1000s of meters.

A solution to the grain boundary issue was first developed by Iijima et al. at Fujikura, in 1991, when it was discovered that oxides, such as yttria-stabilized zirconia (YSZ), could be grown with biaxial texture on untextured substrates by focusing an argon-ion beam at a select angle to a substrate during the vapor phase deposition process [19–21]. The resulting bi-axially textured films had single crystal-like properties and supported the subsequent growth of epitaxial YBCO films with low grain boundary misorientations, enabling high J_c 's. This ion beam assisted deposition (IBAD) process was used for the deposition of biaxially textured YSZ films on flexible metal tapes using a roll-to-roll process, demonstrating the first potential route to manufacturing continuous lengths of a highly textured YBCO films. This discovery reignited research efforts around the world and marks the real beginning of the 2G HTS wire development. The ensuing research rapidly identified alternate paths for producing textured templates and multiple methods for depositing the HTS layer.

5.3 2G HTS Wire—Architecture and Manufacturing Options

The fundamental properties and in-plane texture requirements of the (RE)BCO materials dictate that the conductors be fabricated in the form of a tape rather than a round wire. Thus all second generation wire today is based on a composite tape architecture comprised of a flexible textured template onto which an epitaxial film of (RE)Ba₂Cu₃O_{7-x} is deposited, as shown in Fig. 5.4. A normal metal surrounds the composite tape to provide a low resistance electrical contact with the (RE)BCO

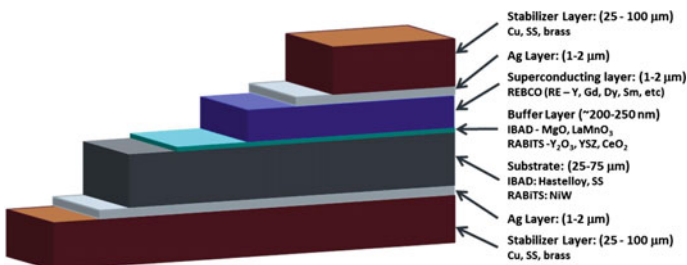


Fig. 5.4 2G HTS wires are manufactured with a composite architecture containing a metal substrate, biaxially textured oxide buffer layers, a biaxially textured (RE)BCO layer, a Ag contact layer and a metallic stabilizer layer (not to scale). Specific materials, formulations and thickness of the individual layers vary from manufacturer to manufacturer (courtesy of AMSC)

and electrical and thermal stabilization for the wire. The template consist of a flexible metallic substrate coated with a series of biaxially textured oxide layers that prevent reaction of the metal substrate with the (RE)BCO and provide a highly textured, single crystal-like surface for the epitaxial nucleation and growth of the (RE)BCO. All commercial 2G HTS wires have this basic composite architecture; however, manufacturers have chosen different technologies to produce the biaxially textured substrates, deposit the HTS layer and stabilize the wire, resulting in variations in the specific materials and architectures of their wires [22].

5.3.1 Template Technologies

The template controls the nucleation and biaxial grain alignment of the (RE)BCO and is the key component that allows roll-to-roll (also referred to as reel-to-reel or R2R) manufacturing of today's 2G HTS wire. In addition to enabling the growth of the biaxial (RE)BCO, the template must also be chemically compatible with the (RE)BCO, stable at the (RE)BCO growth conditions, amenable to formation into tapes and provide sufficient mechanical stability to the thin (RE)BCO films. The three processing technologies used today include the rolling-assisted-biaxially-textured-substrate (RABiTSTM), IBAD and inclined substrate deposition (ISD) processes as illustrated in Fig. 5.5.

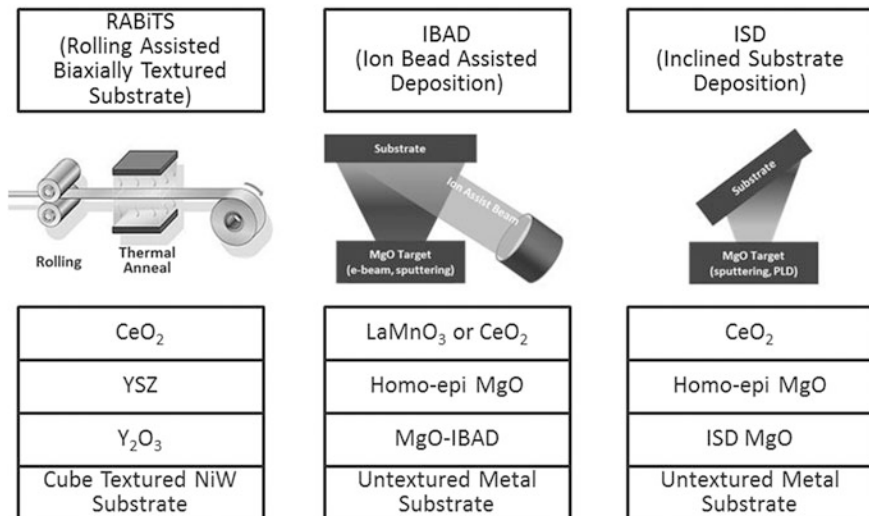


Fig. 5.5 Three basic fabrication methods, **a** RABiTS, **b** IBAD and **c** ISD have been developed for producing templates with high degree of in-plane grain alignment needed high performance and amenable to R2R processing over long continuous lengths

The RABiTS technology (described in greater detail later in the chapter) is based on generating a $\{001\}\langle 100 \rangle$ cube texture in a metal substrate by conventional rolling deformation and recrystallization techniques, as the metal is converted into a thin tape [23–25]. Although many cubic metals or alloys can be textured, face-centered cubic (FCC) materials such as Cu and Ni are the materials of choice since the thermo-mechanical deformation generates a sharp texture in which the cube plane is oriented parallel to the tape plane and a cube edge parallel to the rolling direction. Since the (RE)BCO is not chemically compatible with the metal substrate, it is necessary to deposit a series of epitaxial oxide layers, typically Y_2O_3 /YSZ/ CeO_2 , on the substrate that replicate the substrate texture, provide a metal diffusion barrier and promote the nucleation and growth of the (RE)BCO film [25].

The IBAD process is based on the bombardment of an oxide film during its vapor phase deposition by an off-normal ion beam which sputters away unfavorable grain orientations, promoting the growth of a highly oriented, biaxially textured oxide film on the untextured substrate. Early efforts focused on YSZ [26] and $Gd_2Zr_2O_7$ films [27, 28]; however, the texture evolution was slow, requiring the deposition of thick films resulting in long processing times and low throughput. Most manufacturers using the IBAD process today deposit MgO films in which the biaxial texture develops rapidly, achieving a constant texture within the first 10 nm [26, 29–32]. The IBAD MgO layer is generally capped with a thin homo-epitaxial MgO layer and then either a $LaMnO_3$ or CeO_2 layer which serves as the nucleation layer for the (RE)BCO [33].

The ISD technology, developed by Hasegawa et al. of Sumitomo Electric Industries (SEI) [34], is based on the deposition of an oxide film, typically MgO, at an angle slightly tilted from the plane of the substrate. The texture develops due to a shadowing effect which promotes preferential growth of the MgO along the [001]-axis at an angle tilted slightly from the substrate normal [35, 36].

5.3.2 Superconductor Layer Deposition

Four different deposition technologies are currently used for the superconducting layer: (a) metal organic deposition (MOD), (b) metal organic chemical vapor deposition (MOCVD), (c) pulsed laser deposition (PLD), and (d) reactive co-evaporation (RCE). In addition, a variety of chemical formulations are used for the (RE)BCO layer in order to enhance deposition rates, growth conditions or J_c for each specific deposition technique. A variety of dopants such as RE_2O_3 or $BaZrO_3$ are also frequently added to generate nano-scale defect structures (typically nano-particles or nano-rods) which enhance flux pinning and thus increase the current the (RE)BCO film carries in the presence of a magnetic field [37, 38].

MOD is an ex situ, chemical deposition technique in which a solution-based precursor is coated onto the template and then converted into the (RE)BCO film [39–44]. This process is described in more detail later.

PLD is a vacuum-based, in situ growth process that utilizes a high power excimer laser (KrF or XeCl) to vaporize a (RE)BCO target that deposits from the plasma onto the template as a thin film. The PLD process has produced some of the thickest, highest I_c (RE)BCO films (1400 A/cm-w at 75 K, self-field) reported to date [45, 46].

MOCVD is an in situ deposition process based on the injection of a precursor material into a reactor chamber where it vaporizes and undergoes a pyrolysis reaction as it deposits as a thin film on a substrate [47]. Early MOCVD efforts used solid phase 2,2,6,6-tetramethyl-3,5-heptanedionates as the precursor sources; however, these have been replaced by single source liquid precursors, based on RE, Ba and Cu tetramethyl heptanedionates (tmhd) which have enabled higher rate deposition and improved stability and uniformity [48].

RCE is a thermal evaporation technique developed for the deposition of the epitaxial, multi-component oxide HTS films [49]. The deposition is carried out either by sequential evaporation of a thin layer of the metal components onto the substrate in a low pressure zone followed by oxidation in a high oxygen pressure zone [50–52] or alternately by the co-evaporation of the entire metal film in a single step, forming an amorphous, glassy sub oxide film which is then converted ex situ to the superconducting (RE)BCO phase [53].

5.3.3 *Roll-to-Roll Processing*

2G HTS wire, which consists of a superconductor thin film on a long length flexible substrate, is ideally suited to industrial R2R processing. A major advantage of the R2R manufacturing is the ability to process wide webs of material which can be slit to the final product width at the end of the process. Although R2R processing is a widely used low-cost, high-volume manufacturing technology, it had not been used for manufacturing of flexible electrical materials, especially ones with the stringent biaxial texture requirements of 2G HTS wire. Thus, in addition to developing the basic deposition technologies, the 2G engineering community also had engage equipment manufacturers to design and build R2R tools that could be adapted to the epitaxial deposition processes.

For cost reasons, it was necessary to maximize the process (or deposition) zone area in order to maximize throughput (m^2/h). Two similar, but distinct approaches were developed for the R2R manufacturing of 2G HTS wire. The first is the wide-web process, pioneered by AMSC and the second is a narrow-web, helix process developed by SuperPower, as illustrated in Fig. 5.6. The wide-web process uses a wide substrate (46–100 mm) which is slit to individual wires (up to 24 individual 4 mm wide wires from a 100 mm web) at the end of the process. This wide web approach is advantageous with the RABiTS template technology which can be produced in wide widths and solution based deposition processes which utilize low-cost ovens with long process zones (10 m or greater) enabling high

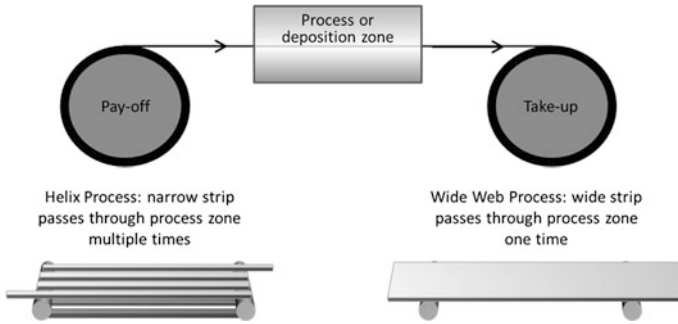


Fig. 5.6 2G HTS wire is manufactured using a R2R process employing either **a** a wide web (50–100 mm) which passes through the deposition or process zone once or **b** a narrow-web (10–12 mm) which passes through a helix deposition or process zone multiple times (courtesy of AMSC)

throughput (m^2/h) compared to PVD systems in which deposition zones are generally restricted to around 1 m.

The narrow-web, helix approach starts with a narrower (10–12 mm wide) strip that is slit into fewer individual wires at the end of the process, or is used without slitting. In order to increase the throughput, the narrow tape passes through the deposition zone multiple times by means of a helix configuration, effectively increasing the length of the process zone. An advantage of the helix system is that inhomogeneities across the width of the deposition zone are averaged out, making it useful for the IBAD template technology and other small deposition area PVD processes such as PLD and RCE depositions.

5.4 AMSC's Selection of the RABiTS/MOD Process Technology

In the early stages of the 2G wire development, it was uncertain whether any template process could achieve the required texture over the hundreds of meter length required for commercial manufacturing or could be done at a cost that would enable a commercial market. In order to identify the preferred manufacturing approaches, AMSC established collaborations through a multi-organizational association called the Wire Development Group (WDG). The makeup of the WDG collaboration varied over the years, but included scientists from Los Alamos National Laboratory, Oak Ridge National Laboratory, Argonne National Laboratory, the University of Wisconsin, the University of California Berkeley, Massachusetts Institute of Technology, Florida State University and Industrial

Research Laboratory (in New Zealand). The WDG collaborators generally focused on a fundamental understanding and the technical capabilities of the different template and HTS technologies, while AMSC scientists and engineers focused on the manufacturability, scalability and cost of the various approaches.

Ultimately AMSC chose the combination of the RABiTS technology for the template and the MOD process for the HTS layer. The primary advantage of the RABiTS/MOD approach is the ability to carry out the entire R2R process using a wide strip which is slit into multiple wires of the desired width at the end of the process. AMSC's current process is designed around a 46 mm wide strip; however, its manufacturing equipment is designed to process strips up to 100 mm wide. A key requirement of the wide-web approach is maintaining uniform properties across the substrate width. Thus in the early 2000s, AMSC focused its early manufacturing development efforts on processing width rather than length, while others, using the narrow-web approach, focused on length. However, once the cross-web uniformity was established on short length strips (~ 100 m), AMSC rapidly extended the length to 500–600 m, which is sufficient for most applications.

In addition to the template and HTS deposition technologies, AMSC uses a lamination process, previously developed for 1G HTS wire, to fabricate the 2G HTS as a robust commercial wire (conductor) for use in a variety of cable and coil applications. In this process, a metal foil is bonded to each side of the slit strip (referred to as the insert wire) and the edges are sealed with solder fillets. The lamination process also provides the flexibility to customize the normal-state electrical or mechanical properties of the final wire for specific applications.

5.4.1 AMSC's RABiTS/MOD Wire Manufacturing Process

AMSC has established a 2G HTS wire manufacturing plant in its Devens, Massachusetts facility based on the RABiTS/MOD process [54]. The facility, designed as a wide-web, R2R process is currently the largest 2G manufacturing plant in the world. Figure 5.7 illustrates the major process steps for the template fabrication, superconductor deposition and wire fabrication. This production line was the result of years of R&D focused on both optimizing the performance of the RABiTS/MOD process and reducing the materials and processing costs. The following sections describe the selected technology in more detail and highlight some of the challenges overcome in its successful development.

5.4.2 The RABiTS Substrate

The RABiTS process was developed by Goyal, et al. at Oak Ridge National Laboratory (ORNL) in the early 1990s and subsequently developed by AMSC into a cost-effective template for 2G wire manufacturing [54, 55]. The basis of the

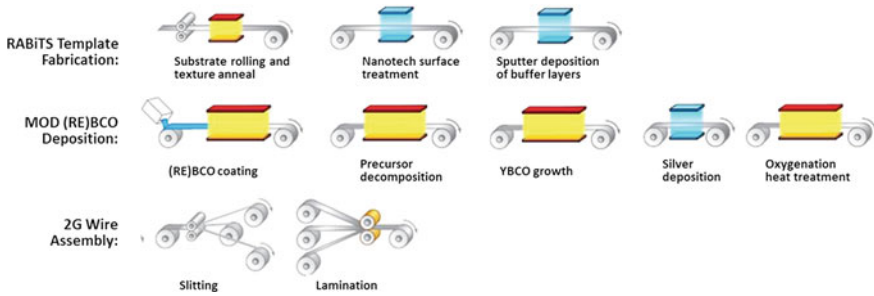


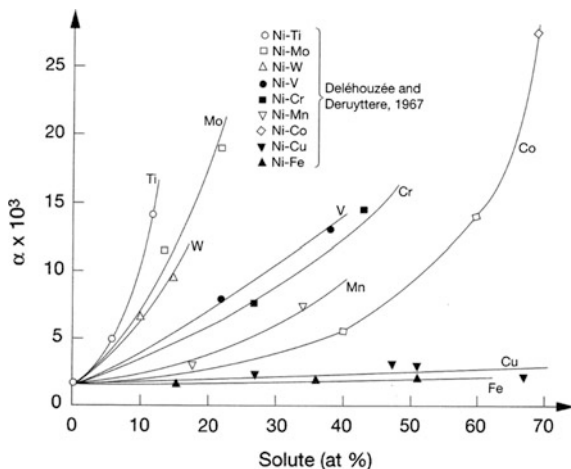
Fig. 5.7 Schematic diagram illustrating basic process steps AMSC uses for the: (1) RABiTS template fabrication, (2) MOD superconductor deposition and (3) final wire 2G wire assembly (*courtesy AMSC*)

RABiTS process is the creation of a thin metallic substrate, with a sharp cube texture, that supports the growth of epitaxial buffer layers [25, 56]. Early R&D at AMSC and ORNL focused on high purity Ni substrates which can be produced with near 100% cube texture. However, pure Ni is very weak when annealed, making the high temperature R2R processing a challenge. In addition, Ni is ferromagnetic, resulting in a hysteretic power loss making it less attractive for alternating current applications. Thus research efforts rapidly focused on identifying suitable nickel alloys that would meet the following substrate requirements:

1. A sharp cube texture in a thin substrate,
2. Non-magnetic,
3. Sufficient yield strength at RT and elevated temperatures, and
4. Oxidation resistance (no native oxide formation at conditions for buffer deposition).

Texture FCC metals with a medium stacking fault energy (SFE) such as Cu or Ni tend to form very sharp, nearly single-crystal like $\{001\}\langle 100 \rangle$ foils when rolled to high reductions ($\sim 95\text{--}99\%$ cube) followed by a high temperature anneal. Although this phenomenon had been known since 1929 [57], it was generally considered a metallurgical curiosity—research often focused on inhibiting texture formation in order to allow isotropic deformation. The capability to form a highly cube textured substrate requires a small grain size at the start of the deformation process, a high deformation strain before final anneal, and a sufficiently high SFE. There are a number of nickel alloys with a medium SFE which are able to develop a cube texture and are oxidation resistant. Figure 5.8 shows the stacking fault probability α ($\alpha = K \cdot \rho/\gamma$), where K is a constant; ρ the dislocation density and γ the SFE, as a function of the concentration of various elements, X , in Ni(X) solid solution alloys [58]. Assuming a constant dislocation density, the data show the inverse SFE has an inverse dependence on X . Trends in Fig. 5.8 were confirmed in a recent modeling study [59].

Fig. 5.8 Stacking fault probability α in Ni(X) solid solution alloys as a function of [X]. $\alpha = K \cdot \rho/\gamma$; K: constant; ρ : dislocation density; γ : SFE. After Gallagher [58]



In Fig. 5.8, the alloys fall roughly into three categories: (1) NiX alloys (Cu and Ni) with a complete or very high solubility and an α nearly independent of composition; (2) NiX alloys (Co, V, Cr, Mn, W and Mo) with a an extensive solubility in Ni and an α that varies with X; and (3) NiX alloys (Ti) with a very low solubility and limited ability to form a sharp cube texture. While Fig. 5.8 shows a gradual decrease of the SFE of these alloys, the ability to form a sharp cube texture does not follow this same dependency. Experience shows that Ni(Cr) forms an excellent cube texture at [Cr] \leq 13 at.%, Ni(V) at [V] \leq 9 at.%, and Ni(W) at [W] \leq 5–6 at.%. However, when [X] exceeds these concentrations, the ability to form a cube texture rapidly deteriorates even though there is only a small additional decrease in γ .

It is also desirable that the RABiTS substrate is non-magnetic (or at least weakly ferro-magnetic) and strong enough to withstand mechanical deformation and damage during high temperature R2R processing. Alloying Ni with metals such as W, Cr, Mo or V significantly increases the strength of the alloy and reduces the Curie temperature. The reduction in Curie temperature in Ni(X) is virtually linear with both [X] and its valency [60], with Cr being nearly 3 times and W nearly 5 times more effective than Cu. For the substrate to be non-magnetic at low temperatures (<20 K), requires approximately 13 at.%Cr, 9 at.%V or 9.3 at.% W.

Oxidation resistance of the alloy needs to be sufficient to withstand processing, in a high temperature, oxidizing environment in subsequent steps, with minimal oxide scale formation. Although elements such as Al provide excellent oxidation protection via the formation of an oxide film (i.e., Al_2O_3), the oxide its formation prior to the buffer deposition will disrupt the epitaxial growth of the buffer layers (this is discussed in more detail in the following section). Other alloying elements that can meet this requirement include W, Mo and Cr.

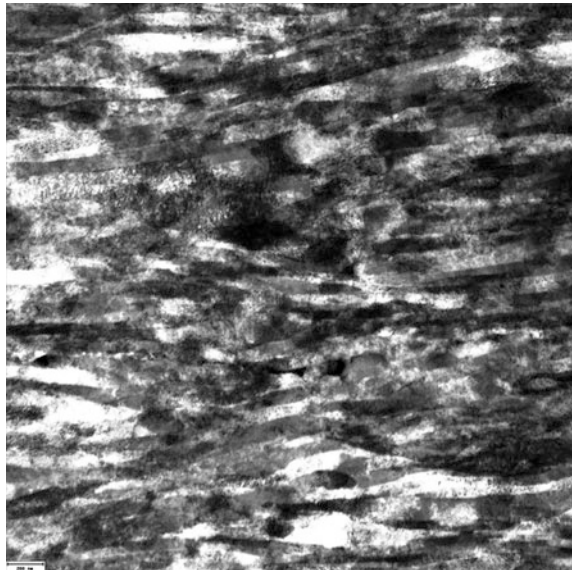
Based on these requirements and suitability for supporting the epitaxial buffer growth, NiW was identified as the best choice for development of the RABiTS substrate. The cube texture forms at W concentrations of up to \approx 5.5 at.% even

though the change in SFE is gradual over the entire 0–10 at.% W. However, at $[W] > 6\%$ the cube texture rapidly decreases. The reason for this abrupt decrease in texture in alloys with lower γ was poorly understood. Thus, although the Ni–5 at.% W is weakly ferromagnetic, AMSC and others chose to work with the Ni–5 at.% W composition since this was initially thought to be minor disadvantage to final wire properties. However, since the competing IBAD template technology is based on a non-magnetic substrate, 2G wire based on Ni–5 at.%W was at a competitive disadvantage in ac cable applications where the ferro-magnetism contributes to enhanced ac losses. As a result, AMSC and others [61] began to study the deformation mechanisms in the lower γ alloys This multi-year research effort eventually led to the development of a proprietary thermo-mechanical process to that produces an excellent cube texture in the non-magnetic Ni–9 at.% W alloy that matches that in the Ni–5 at.% W composition.

Detailed studies of the microstructure development in both the Ni–5W and Ni–9W alloys showed them to be similar to those of FCC alloys with a medium SFE [62]. After an initial stage of deformation banding, highly distorted lamellae develop and evolve into a structure of nearly horizontal but wavy, in-plane lamellae, as shown in the transmission electron microscopy (TEM) micrograph in Fig. 5.9.

Figure 5.10 shows the texture components M_i for substrates rolled to final thickness ($\eta = 3.9$) (prior to the final thermal anneal) for Ni–5W and Ni–9W, with the standard and the modified thermo-mechanical process, respectively. Ni–5W texture components are similar to that of pure copper.

Fig. 5.9 TEM image of rolled Ni–9W, thickness is 0.076 mm. Longitudinal view, rolling direction is horizontal; Bar in *left corner* 200 nm. V. Svetchnikov and C. Tretiatchenko, Institute for Metal Physics, Kiev



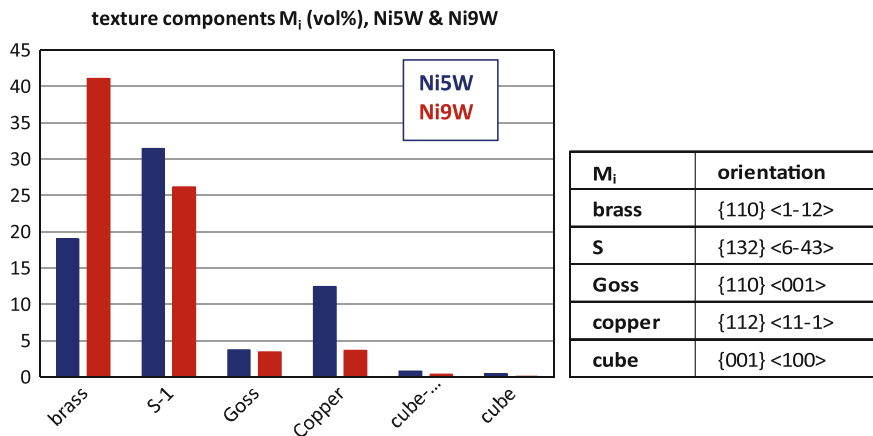


Fig. 5.10 Texture components M_i (vol.%) for Ni–5W and Ni–9W at final thickness (FWHM: 10°)

As seen in Fig. 5.10, the S texture $\{132\}\langle 6-43 \rangle$ is the strongest component in the Ni–5W composition, followed by the brass orientation $\{110\}\langle 1-12 \rangle$, copper $\{112\}\langle 11-1 \rangle$ and Goss $\{110\}\langle 001 \rangle$. The $\{001\}\langle 100 \rangle$ cube and cube-Goss $\{025\}\langle 100 \rangle$ components are 1% or less. In contrast the Ni–9W composition shows a very different picture with the brass texture being the dominant component, followed by S, Goss and a relatively low copper component. In both compositions Cube and Cube-Goss textures are well below 1%. However, despite these quite dissimilar M_i (% texture component) values the final textures for the Ni–5W and Ni–9W are very similar (97–98% cube).

Figure 5.10, in which the final desired cube orientation is nearly absent, does not foretell the formation of a near 100% cube texture during the final anneal in any way. This example illustrates the difficulty in pin-pointing the exact stabilization and growth mechanisms for the few existing cube lamellae in the final substrate. For a review of the theory (and historical background) of cube recrystallization texture see for example Humphreys and Hatherley [63]. It is generally believed that high angle boundaries combined with strain-induced boundary movement (SIBM) is essential in cube growth. Already existing, stable cube lamellae grow into the neighboring lamellae with a different texture, in which particular grain boundary orientations can assist in this growth. The low concentration of cube lamellae, as found in NiW can be advantageous, since higher levels can block growth when cube growth bands “collide” leading to orientation pinning as has been observed, for example, in Al. However, to track this process in Ni–9W and be more precise about the growth of the cube texture extensive high resolution scanning electron microscopy (HRSEM)/TEM combined with electron backscatter diffraction (EBSD) analysis is still required at various stages of the growth process.

Long Length RABiTS Substrate Manufacturing AMSC worked closely with collaborators at ORNL to scale the RABiTS process from the initial short sample demonstration to a wide-web R2R process. The major effort focused on developing the appropriate deformation and annealing paths to insure a sharp and uniform cube texture was generated over both the width and length of the substrate. With the optimized deformation and annealing process, a cube texture of 96–98% is achieved over the length and width of the substrate. The cube texture is determined from the integrated area of the (200) or (111) X-ray pole figures and full width at half-maximum (FWHM) values for in-plane ($\delta\phi$) and out-of-plane ($\delta\chi$ and $\delta\omega$) texture.

The measured in-plane texture, $\delta\phi$, values, which are averaged over a large area, are between 6.5–7°. Although this is larger than the 4° grain boundary mis-orientation that Dimos showed caused a precipitous drop in supercurrent, these substrates support currents in the (RE)BCO layer of >4 MA/cm². One reason for the higher than predicted J_c is an improvement of the in-plane texture, $\delta\phi$, of the initial Y₂O₃ buffer layer. This sharper Y₂O₃ texture is inherited by the subsequent YSZ barrier and CeO₂ cap layer (see later section). Secondly, in the MOD (RE)BCO layer the grain boundaries are typically slanted and meandering, enhancing the total grain boundary (GB) area available for current transport [64].

It is also critical to prevent the formation of other texture components which can appear as obstacles to the super current flow. For example, annealing twins form high angle grain boundaries with the cube texture grains and abnormal grains, which can reach 200–300 μm in size, and appear as obstacles to the supercurrent flow.

In the early development, texture uniformity was examined by scanning the length and width of the substrate using a R2R x-ray analysis system at ORNL. However, the best indicator of texture homogeneity is the local and long-length uniformity of the supercurrent along the length of each individual wire produced from the RABiTS substrate.

The initial development efforts used small (~20 lb.), high purity, laboratory scale Ni–5 at.% W ingots which can prepared with precisely controlled compositions, typically within 0.1 at.%. However, a commercial manufacturing operation requires multi-ton quantities with the same purity and homogeneity requirements. AMSC worked closely with metal suppliers to develop a production scale process based on a conventional melt of high purity Ni and W followed by a second melt to remove volatile impurities. The melting process is followed by a homogenization treatment, a hot deformation step and cold rolling to desired thickness, with anneal steps at critical stages. This process routinely yields high purity, compositionally homogeneous Ni–W coils which can be used for precise rolling to final thickness, and slitting to desired width. A similarly scaled process has now also been demonstrated for the non-magnetic Ni–9W alloy, on which superconductors have been demonstrated in length, and with critical currents approaching those on Ni–5W.

5.4.3 *Epitaxial Growth of Oxide Buffer Layers on NiW Substrates*

Buffer layers play several key functions on the RABiTS template including:

- (1) Transfer of texture from the metal substrate to the (RE)BCO layer,
- (2) A chemically inert surface for the nucleation and growth of the (RE)BCO,
- (3) A barrier to prevent metal diffusion from the substrate to the (RE)BCO layer during the high temperature growth,
- (4) A barrier to prevent oxidation of the metal substrate during processing, and
- (5) Provide mechanical stability and adhesion of the (RE)BCO layer to the substrate.

To accomplish all these functions, the buffer layers must be matched as closely as possible in both the lattice parameters and the coefficient of thermal expansion to the alloy substrate and the (RE)BCO film. The buffer layers also need to be continuous, smooth, crack-free and dense, to provide effective chemical separation between the alloy substrate and the HTS film. Any contamination of the (RE)BCO layer with the elements from the substrate can degrade the superconductivity of the (RE)BCO materials. For instance, as little as 3% Ni substitution in the Cu site in YBCO reduces the critical temperature to below 77 K [65].

AMSC and collaborators at ORNL explored a variety of materials that would meet all of the buffer layer requirements and ultimately settled on a three layer combination of Y_2O_3 /YSZ/ CeO_2 deposited by physical vapor deposition (PVD), in particular by reactive magnetron sputtering. A cross-section TEM image of the buffer stack in a fully processed conductor is shown in Fig. 5.11, along with a table of typical values of the full width at half-maximum (FWHM) of the out-of-plane texture, $\Delta\chi$ and in-plane texture, $\Delta\phi$ peaks illustrating the sharpness of the texture in each of the layers. In this stack, each layer performs a distinct function. The Y_2O_3 layer deposited directly on the Ni-W substrate acts as a seed layer that replicates the texture of the Ni-W substrate, the YSZ functions as a barrier layer to prevent the diffusion of Ni and W to the (RE)BCO and CeO_2 serves as a “cap” layer which provides an optimized surface for the nucleation and growth of MOD-(RE)BCO. As shown in the table in Fig. 5.11, the Y_2O_3 seed layer has a significant sharpening of the texture over that observed in the Ni-W substrate, and this sharpness carries through to the YSZ and the CeO_2 layers. The texture sharpening, which is unique to the PVD Y_2O_3 layer is believed to arise from lattice strain introduced during the deposition process.

A variety of deposition techniques were explored for the epitaxial deposition of the buffer layers on the NiW RABiTS substrate. These include vacuum based processes such as PLD [66, 67], electron beam evaporation [68], MOCVD [69], rf and reactive sputtering [70–73], etc., and non-vacuum processes such as chemical solution deposition [74, 75]. Among these synthesis methods, chemical solution deposition is the most cost-effective, but sputtering yields the best quality film at reasonable rates to make it manufacturing-friendly.

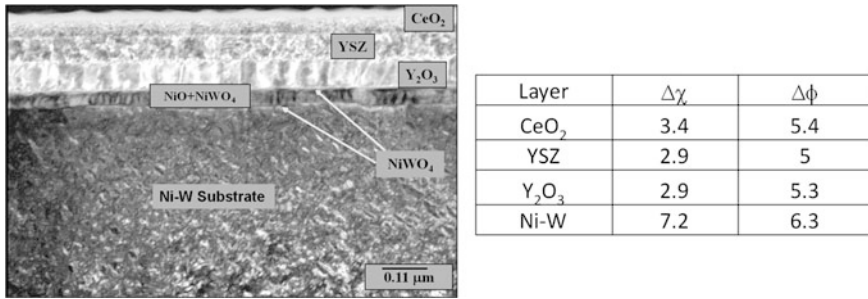


Fig. 5.11 Cross-section TEM of fully buffered RABiTS after (RE)BCO processing showing the three layer buffer architecture along with a thin layer of adherent native Ni-W-Oxide formed during (RE)BCO processing. The *table* shows typical texture (FWHM) of the substrate and the three buffer layers

In the early R&D development, AMSC used rf-sputtering to deposit the oxide buffer layers. Although rf-sputtering of metal oxides produces highly textured, dense, films with excellent stoichiometry control and is applicable to a wide range of material compositions, the deposition rates are low since the low thermal conductivity of the oxide targets limits the plasma energy that can be used [25]. To circumvent this rate limiting problem, AMSC used reactive sputtering for the manufacturing process. In the reactive sputtering process, thin films of compounds are deposited on substrates by sputtering from metal targets in the presence of a reactive gas (H₂O, oxygen or nitrogen) usually mixed in with the process gas (such as Ar). Careful control of the reactive gas pressure in the sputter atmosphere is critical to controlling the film stoichiometry and the sputtering rates. While the stoichiometry control and the film densities for reactive sputtering are slightly inferior to rf-sputtering of oxide targets, the enhanced deposition rates accommodated by reactive sputtering make it a very attractive industrial process.

Deposition of Seed Layer One of the biggest materials challenges in the RABiTS template development was the deposition of the seed layer on the textured Ni-W alloy substrate. The primary role of the seed layer is to provide an ideal surface for the nucleation and growth of subsequent oxide layers while providing a perfect transfer of the biaxial texture in the Ni-W alloy. The vapor phase deposition of the metal oxide seed layer such as Y₂O₃ by reactive sputtering is typically carried out at a high temperature in the presence of oxygen, conditions which favor the formation of the native oxides of the Ni-W substrate.

A clear understanding of the stability regimes of these oxides relative to those of the oxides of Ni and W is essential. The Ni in the substrate oxidizes at a pO₂ higher than 10⁻¹² mTorr, and the W oxidizes at a pO₂ higher than 10⁻¹⁴ mTorr. Any oxidation of the substrate disrupts the epitaxial nucleation of the seed layer leading to a degraded or random texture which propagates through the next layers. Hence, one of the key requirements of materials choice for a seed layer is the ability to nucleate and grow as a stoichiometric oxide at oxygen pressures where the substrate

components are thermodynamically stable. Y_2O_3 or CeO_2 are typically grown in a H_2O/H_2 atmosphere that produces an effective pO_2 in which Ni and W are stable against oxidation but the Ce and Y oxides are stable. In contrast, these materials cannot be grown on NiCr substrates since the Cr oxides are stable at much lower oxygen pressures than the Y and Ce oxides.

Based on the initial success in depositing epitaxial layers of CeO_2 or Y_2O_3 on Ni-based substrates, AMSC began developing the full buffer stack. However, it was found that occasionally, Y_2O_3 layers would nucleate c -axis oriented but with multiple in-plane textures. Around the same time, Cantoni et al. showed that the formation of a sulfur superstructure on the metal alloy surface promoted the formation of a single in-plane texture with these seed layer materials [76–78]. Using reflection high energy electron diffraction (RHEED) to monitor the nucleation and growth of epitaxial oxide films on textured Ni-substrates, they observed the formation of a $c(2 \times 2)$ sulfur superstructure on the textured Ni surface, prior to the nucleation of the epitaxial oxide as illustrated in Fig. 5.12. The $c(2 \times 2)$ type superstructure was found to provide a template which promoted the a single in-plane nucleation of the oxide seed layer as schematically illustrated for YSZ nucleation in Fig. 5.12. This $c(2 \times 2)$ superstructure, identified by Cantoni, formed as sulfur impurities in the Ni diffused to the surface as the substrate was heated in the PVD deposition process. Since the impurity level of S varies in the starting Ni material, this explained the variation AMSC observed in the early development work.

This groundbreaking work by Cantoni clearly showed the critical role the nano-scale substrate surface structure plays in controlling the epitaxial nucleation of these oxide layers. Such precise control of the surface structure posed a challenging

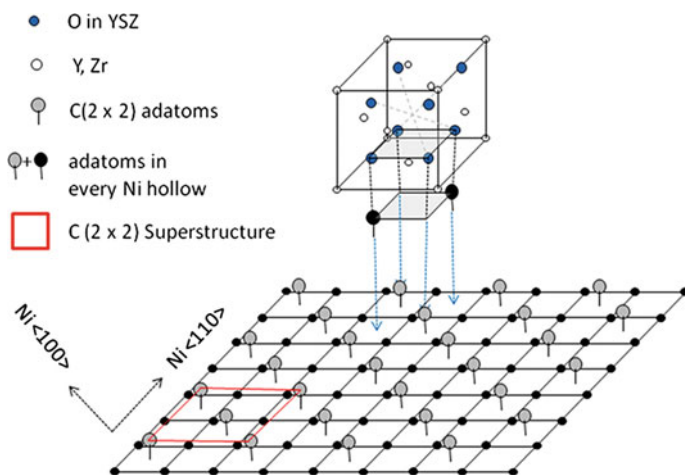


Fig. 5.12 Schematic illustration of a $c(2 \times 2)$ superstructure formed by adatoms mediating epitaxial growth of YSZ on (001) Ni surface (Based on model proposed by Cantoni et al. (based on Fig. 4 in [76])

problem in the R2R deposition process in which the nano-structure needs to be controlled over hundreds of square meters of substrate. The solution was a precise control of the impurity levels in the starting substrate material and development of a proprietary process that promotes a controlled, highly reproducible surface structure during the sputtering process over long lengths.

Once the importance of the nano-surface structure of the substrate was fully understood and processes were developed to precisely control $c(2 \times 2)$ superstructure, development of the YSZ barrier and CeO_2 cap layers were straight forward processes.

5.4.4 *Epitaxial Growth of Thick YBCO Films*

AMSC chose to develop the trifluoroacetate-based (TFA) MOD process rather than a vacuum-based approach for the superconductor layer since solution-based routes are significantly less expensive, the precursors are inexpensive with utilization rates of nearly 100% and the process can be readily scaled for a wide-web process. The TFA precursor was selected since the intermediate formation of BaF_2 during the processing prevents the formation of BaCO_3 which collects at grain boundaries, limiting the current in the final HTS film. Although solution-based coating processes are widely used in industry (i.e., photographic film, papers, etc.), they had never been used for the continuous deposition of thick, epitaxial, high quality electronic ceramic films over flexible, kilometer-length substrates. Thus, AMSC faced significant technical challenges to both develop the process and design the equipment necessary for low-cost manufacturing. AMSC's implementation of these processes is described below.

Precursor The TFA-based precursor was originally developed by Gupta et al. [39], and later refined by McIntyre et al. [40, 42], to avoid the formation of the stable BaCO_3 during the pyrolysis of the organic components. During the pyrolysis process, the thermodynamically stable barium oxyfluoride phase is formed rather than the detrimental BaCO_3 , which is converted to the oxide by reaction with H_2O .

The original precursor was based on a methanol solution of the Y, Ba and Cu trifluoroacetate salts; however, AMSC made modifications, as discussed below, to increase the film thickness and reduce the processing time. In addition, composition changes were made to promote the formation of nanoparticles throughout the film and increase the flux pinning. AMSC's current precursor consists of a proprietary alcohol-based solution of Y, Dy, Ba and Cu trifluoroacetates and carboxylates along with a stabilizer.

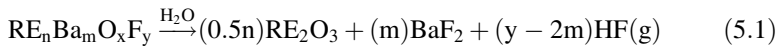
Coating and Pyrolysis A standard industrial slot-die coating process was developed for coating the precursor on the RABiTS template. In the slot-die technique, a metered amount of precursor is dispensed on a moving template which is then passed into a low temperature oven to remove the solvent. This technique produces

a film with excellent thickness and compositional uniformity over the length and width of the template and excellent control of run-to-run variability.

The organic components of the dried film are removed in a separate pyrolysis process carried out in a moist oxygen atmosphere at a temperature around 400 °C, leaving a film comprised of copper oxide and RE-Ba oxyfluoride ((RE)BaOF) phases. The pyrolysis reduces the film thickness by over 50%, and generates extreme stress in the film which can lead to cracking and delamination. Additionally, gas evolution can also lead to blistering and film failure. In order to eliminate these defects, the original decomposition process, developed by McIntyre et al. [40, 42], required over 15 h to produce a 200 nm thick film on a small ($\sim 1 \times 1$ cm) single crystal substrate without defects.

Such long processing times and thin films are not compatible with high-rate, low-cost R2R manufacturing of high performance (thicker) films on long length flexible substrates. Thus AMSC focused on understanding the stress formation mechanisms throughout the pyrolysis process and subsequently modified the copper and rare earth chemistries to mitigate the stress, control gas evolution and accelerate the process time [41, 79–84]. These changes in the chemistry have enabled the routine deposition of films with a thickness of 1.2 μm (effective thickness of a 100% dense (RE)BCO film) with a total pyrolysis time of less than 1 h.

Reaction The decomposed metal oxyfluoride film is converted to the (RE)BCO phase by reaction with H_2O and O_2 according to (5.1) and (5.2):



Since the (RE)BCO film must grow epitaxially, it is necessary that the initial nucleation occur at the textured template (CeO_2) surface within a narrow temperature range. The epitaxial growth then proceeds through the thickness as illustrated in Fig. 5.13 [81, 85]. During the growth process, untextured rare earth based nanoparticles, which are important for pinning (see below), must also form uniformly throughout the film thickness without disrupting the epitaxial (RE)BCO growth. As observed in the SEM images in Fig. 5.13, the film thickness reduces over 50% during this process. In order to insure the proper epitaxial growth, it is necessary to precisely control the (RE)BCO nucleation and growth kinetics, which depends on the equilibrium $K_{eq} \triangleq [\text{HF}]^4/[\text{H}_2\text{O}]^2$. Achieving a uniform growth rate requires precise control of the $\text{H}_2\text{O}(\text{g})$ and $\text{HF}(\text{g})$ concentrations at the tape surface along both the length and width of the tape. With a short, stationary sample this is a relatively easy process; however, in a wide-web, R2R process it is a more challenging issue since the HF evolution changes along the length of the furnace and mixes with the process gas as it flows through the furnace [41]. If the $[\text{HF}(\text{g})]$ varies across the width of the web, the nucleation and growth rate will be affected,

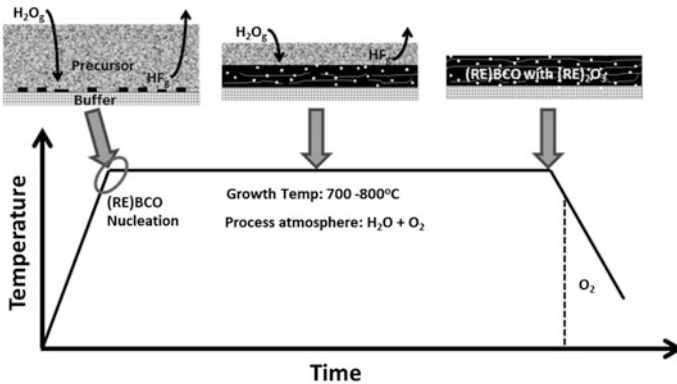


Fig. 5.13 Schematic illustration of the nucleation and growth of the (RE)BCO phase and RE_2O_3 nanoparticle formation as a function of temperature and process gas

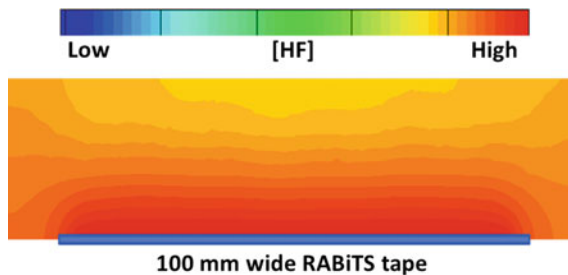


Fig. 5.14 Computational fluid dynamic model showing the $HF(g)$ concentration across the width of a 100 mm wide MOD coated (RE)BCO RABiTS tape in the nucleation zone of the (RE)BCO growth process

resulting in an inhomogeneous (RE)BCO grain structure and subsequently large variations in the I_c of the HTS film. The solution to this challenge was a detailed study of the nucleation and growth kinetics and the use of computational fluid dynamic modeling, to design a 10 m long furnace in which the O_2 , H_2O and HF concentrations can be independently and precisely controlled over both the width and length of the moving tape. Figure 5.14 shows the uniformity in the calculated $[HF]$ concentration across the width of a 100 mm wide tape in the nucleation zone of a 10 m furnace. This approach has allowed the design of production scale furnaces that achieve growth rates exceeding 10 \AA/s over the entire width of the wide-web RABiTS templates.

MOD has some advantages in the way grain-growth occurs, particularly when high angle grain boundaries are present in the RABiTS template. Unlike the vacuum-based growth processes, which have a columnar type growth of the (RE)

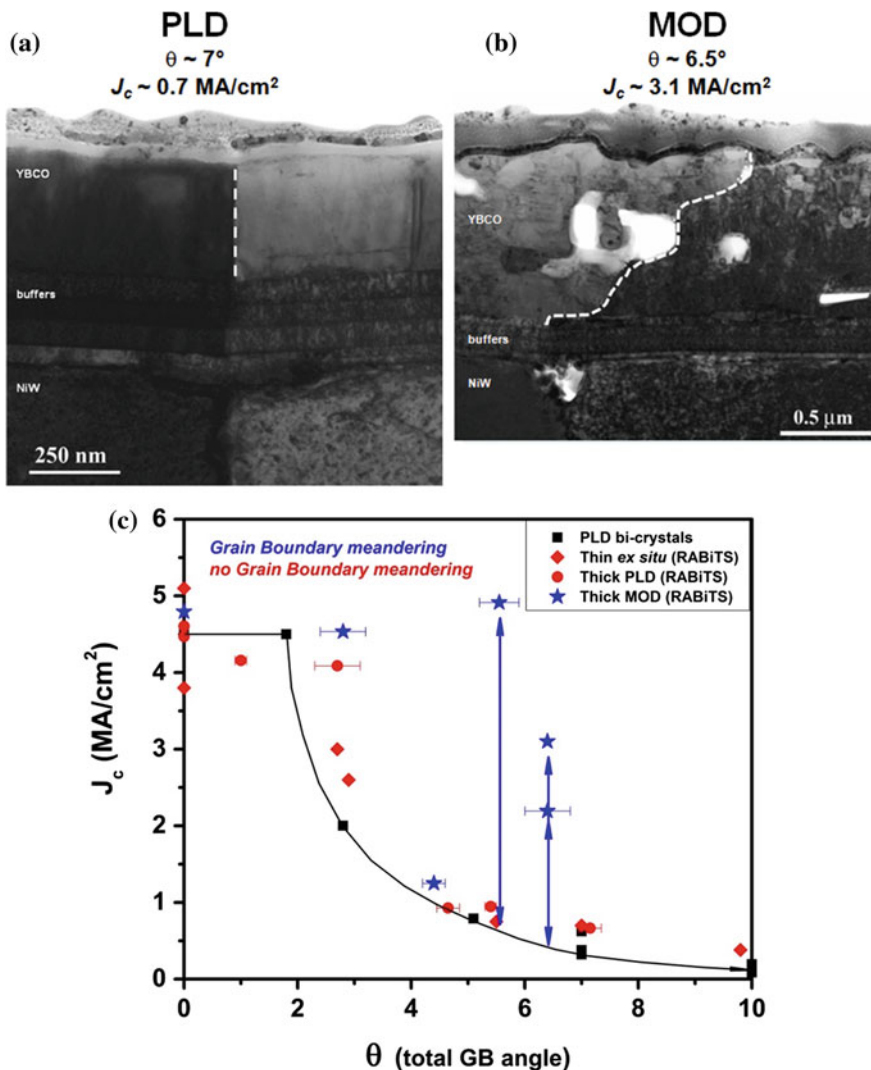


Fig. 5.15 TEM image of the growth modes of **a** PLD and **b** MOD (RE)BCO films across high angle boundaries and **c** the benefit of meandering grain boundaries on J_c [64]

BCO, the MOD process has a lamellar type growth (as shown in Fig. 5.15a, b) [64]. This lamellar growth allows the (RE)BCO grains to meander over the template grain boundaries, particularly as the film thickness increases. Figure 5.15c shows that the meandering grain boundary of the MOD (RE)BCO at least partially negates the current blocking effect of the high angle RABiTS template grain boundary, whereas the PLD (RE)BCO with the columnar grains shows a significant decrease in J_c across a similar grain boundary as predicted by the Dimos plot [17].

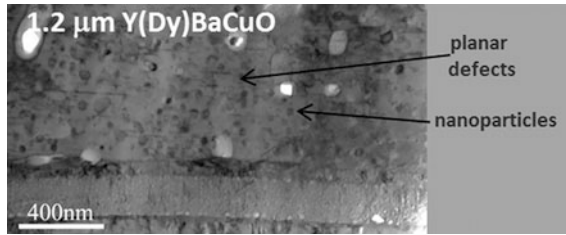


Fig. 5.16 Cross-sectional TEM micrograph of a 1.2 μm thick Y(Dy)BCuO film deposited by the MOD process developed by AMSC

After the formation of the (RE)BCO phase, a thin Ag layer is deposited on the YBCO surface to provide passivation and a low resistance electrical contact, and then the (RE)BCO film is heated in an O_2 atmosphere to oxygenate the (RE)BCO, thereby forming the orthorhombic superconducting phase.

The final HTS layer, shown in the TEM image in Fig. 5.16 consists of a (RE) BCO matrix containing a uniform distribution of rare earth-based nanoparticles which pin magnetic flux lines and so enhance the critical current in the presence of magnetic fields oriented perpendicular to the tape surface, and also a distribution of planar defects that enhance the critical current in magnetic fields oriented in the plane of the tape.

5.4.5 Wire Fabrication

The last step in the 2G HTS wire manufacturing process is to convert the wide web into individual narrow wires. This is done by roll slitting (Fig. 5.6) the wide strip into multiple strips of generally 4–10 mm width, depending on the application. These individual strips are then laminated (Fig. 5.6) between two metal strips to form a robust, hermetically sealed composite wire architecture, shown in Fig. 5.17, that is impervious to environmental degradation; electrically stable during quenches and mechanically strong enough to withstand the rigors of the cable and coil fabrication processes, repetitive cooling and heating cycles, and the stresses experienced in application [86].

The lamination process also provides the flexibility to customize the electrical or mechanical properties of the final wire depending on the material chosen for the metal strips. Typically, high conductivity copper is used for wire intended for conduction-cooled lower temperature coil applications, while brass and stainless steel are favored in liquid nitrogen ac applications such as cables and resistive fault current limiters [87], respectively. In AMSC's 2G HTS wire, which uses a Ni–5 at. % W or Ni–9 at. % W substrate, the mechanical properties are predominantly determined by the properties of the lamina and solder fillet dimensions.

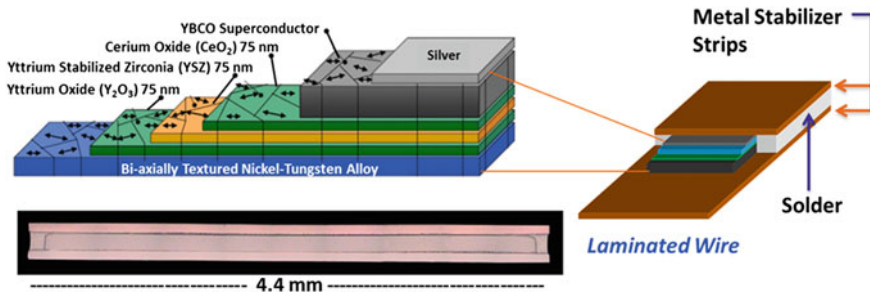


Fig. 5.17 Schematic illustrations of AMSC's 2G insert and laminated wire architectures. A TEM micrograph of the insert cross-section is shown in the *upper right* and an optical micrograph of a cable wire transverse cross-section is shown in the *bottom left* (courtesy AMSC)

5.5 On-Going R&D

The performance of today's 2G HTS wire is suited for several applications, but broad market penetration of this technology necessitates that the cost associated with these materials be reduced. Therefore, most of the R&D focus at AMSC revolves around various approaches to reduce the effective wire cost or price-performance metric, measured in \$/kA-m (dollars per kiloampere-meter). The main areas of focus include increasing capacity (to drive down manufacturing cost through volume production), increasing performance and developing more cost-effective deposition technologies.

With an eye toward high capacity manufacturing, right from the outset of this technology, AMSC has focused on a wide-web manufacturing approach. In the early days of scaling up the RABiTS process, AMSC's R&D focused not only on processing longer strips, but also wider strips. This approach lends itself to capacity expansion without significantly increasing the equipment footprint or capital equipment cost. The AMSC process has moved from the initial 1 cm wide strips, which are still used by some manufacturers, to the current 4.6 cm wide strips which are slit to the required wire widths. The next step in this scale-up will be a 10 cm wide strip for which all the process equipment currently in use is designed to handle, and long term R&D will focus on increasing the strip width further. The increased capacity provides a pathway to meet the demands of large projects that require large quantities of wire, and as the quantities of wire being used increases, the cost will naturally come down.

Any improvement in critical current directly affects the effective cost of the 2G HTS wire to the customer, as it reduces the amount of wire required to build a device. The improvements are not focused just on the 77 K $sf I_c$ but also at the operating temperatures in the 4–50 K range in a few tesla magnetic field. In the last

few years, significant improvements have been achieved in the performance of commercial long length wires with the I_c more than doubling in the 4–50 K range. Additional increases in performance will come from a combination of enhanced pinning through skillful engineering of the pinning microstructure, and increases in thickness of the HTS layer.

Most of the improvements in pinning in all the different superconductor deposition methods have resulted from the introduction of correlated defects, oriented along the c -axis, and point defects. These have been accomplished using introduction of twin boundaries, addition of nanoparticles in the HTS layer, introduction of ab -planar defects, and in situ growth of BaZrO₃ or BaHfO₃ nano-columns [88]. These approaches to engineer the pinning microstructure have been particularly effective to enhance properties at low temperatures and high fields, with wire performance approaching 1000 A/cm-width in magnetic fields ($H//c$) around 2T at 30 K. Controlling these nano-scale engineered pinning microstructures over kilometer lengths of wire processed is still a manufacturing challenge.

While these recent advances are being transferred to the manufacturing lines, other avenues for additional flux pinning enhancement are continuously being explored. One area that has shown promise is irradiation by ions ranging from protons to gold [89]. Recent work has shown that such irradiation processes can more than double the critical current of 2G HTS production wire at temperatures and fields relevant to rotating machines, while adding minimal cost to the wire [90].

Another potential area of cost reduction is the development of solution-based buffer layers for the RABiTS substrates. Solution processing is an inherently high volume low-cost approach which is compatible with the wide-web manufacturing used at AMSC. The process offers significant advantages over the PVD processes currently in use, such as 100% material utilization, fast coating rates, uniform coating thickness over large widths, and no need for expensive high vacuum equipment. The feasibility of this approach has already been demonstrated with reasonable success for the barrier layer using lanthanum zirconate [91]; however, the development of a solution-based seed and cap layers is still at a very early stage. In case of the seed layer, the PVD Y₂O₃ seed layer shows an enhancement in texture over the metal substrate. The fundamentals of epitaxial nucleation that contribute to this phenomenon are not fully understood at the current time. The challenge for a solution-based process would be to produce similar texture improvements, and that has only been partially demonstrated with lanthanum niobate and lanthanum tantalate films [92]. In case of the cap layer, the PVD CeO₂ has been tailored to be ideally suitable for the nucleation and growth of the MOD-HTS layer. The solution processed CeO₂ layer, while epitaxial, has yet to demonstrate that kind of suitability. Additional R&D is required to fill these rather large gaps in understanding for solution buffers to become a viable cost-cutting alternative in 2G wires.

5.6 2G HTS Wire Manufacturers, Wire Market and Needs

Over 25 years after the discovery of the HTS materials, 2G HTS wire is ready to be deployed in the first commercial applications and begin to fulfill the promise of a revolution in the way electricity is generated, delivered and consumed. Although the development of the HTS wire technology has been a long path, it is similar to other revolutionary, high-risk material-based technologies, such as optical fibers and semiconductors, which required two or more decades to move from the laboratory to the commercial market.

Today there are around 10 commercial companies involved in manufacturing of 2G HTS wire, as shown in Fig. 5.18. AMSC and SuperPower (now fully owned by Furukawa) have established manufacturing facilities and have produced most of the 2G HTS wire used to date. The other companies are either in the early stages of establishing manufacturing facilities or still developing the processes.

The applications for which 2G HTS wires are targeted can be separated into two groups. The first includes existing applications, such as cables, motors, generators, transformers and magnets, where 2G HTS wire replaces conventional resistive copper conductors. The second group encompasses new technologies that cannot be addressed with conventional conductors, such as superconducting fault-current limiters (SFCLs), superconducting magnetic energy storage (SMES) and certain defense applications. Penetrating an existing market is challenging and requires that the 2G HTS wire has both a performance and economic advantage over the established conventional technologies. Although today's 2G HTS wire can meet or exceed the performance requirements for many applications, the cost of the wire



Fig. 5.18 2G HTS wire manufacturing is being pursued by companies in the United States, Europe and Asia. Most commercial wire has been produced by AMSC and SuperPower, while the other companies are either in the early stages of establishing manufacturing facilities or still developing the manufacturing processes

still leaves it at an economic disadvantage in many cases. However, as the manufacturing capacity ramps up, manufacturing capability improves and performance continues to increase, this economic difference is beginning to decrease.

In contrast, new applications, for which there are no conventional solutions, are less sensitive to cost concerns and are likely to be the first products accepted in the commercial market. As these markets evolve, they will help drive down the cost of the 2G HTS wire to a level where it can compete with established technologies.

AMSC has chosen to focus in the near-term on providing wire to applications in the electric utility and defense areas where the value-proposition of the HTS system is compelling. Brief descriptions of the major applications AMSC is pursuing are described below.

5.6.1 Fault Current Limiters

Current surges or fault currents in the electrical grid are becoming more common and destructive, particularly in urban areas, as new power generation sources are added to meet the world's growing energy demands. As the severity of these fault currents increases, they are approaching levels that exceed the safe operating limits of conventional circuit breakers and other grid equipment.

The unique properties of 2G HTS wire have allowed the development of a SFCL technology that effectively addresses this problem [93–96]. In the “resistive” SFCL (the most common design), a fault current (one exceeding the critical current) instantly forces the HTS wire to transition to a very high resistance state, effectively shunting the current into a higher resistance layer, thereby reducing the amplitude of the fault current. Once the fault current is cleared, the 2G HTS wire-based SFCL returns to its normal superconducting state and is ready for the next fault. AMSC manufactures a customized FCL wire that utilizes a high resistance stainless steel laminate to optimize the wire's overall resistance and its capacity to absorb heat generated during the fault. Alternate SFCL designs, based on inductive concepts are also being developed.

Although SFCL's not are a huge volume market for 2G HTS wire, they are anticipated to be one of the first products installed in the commercial electrical grid. Currently SFCL systems, based on AMSC's 2G HTS wire, are available from Nexans [97].

5.6.2 Cables

Compact, high-efficiency, HTS-based power cables are envisioned as an important new technology for boosting grid capacity and transmitting large amounts of electrical power over long distances and represent one of the largest potential commercial markets for 2G HTS wire. The engineering critical current density (J_c) of today's 2G HTS wire is nearly 100 times greater than that of conventional copper

conductors; thus HTS power cables can carry several times as much power as conventional copper cables of the same size. Additionally, since HTS-based cables do not produce the resistively generated heat or strong electromagnetic fields associated with conventional copper cables, they can be readily installed in compact spaces near other underground infrastructures. For this reason, 2G HTS cables are viewed as a near-term, cost-effective solution for delivering power over short distances in congested urban areas where the right-of-way is limited and siting and installation of conventional cables is expensive and difficult.

The technical feasibility and reliability of HTS-based cables has been demonstrated in a number of government supported projects around the world over the past decade, with the longest being a 1 km, 10 kV, 40 MVA cable, based on 1G HTS wire, installed by Nexans, Karlsruhe Institute of Technology and RWE in Essen Germany and energized in May 2014 [98–103].

AMSC, Southwire, Consolidated Edison and ORNL, with support from the U.S. Department of Homeland Security, have developed a novel fault-current limiting cable technology that combines the high current capacity of a HTS cable with inherent FCL functionality [104, 105]. This unique technology provides a means to increase the resiliency of the electric grid to disruptive faults (from either natural causes or intentional acts of vandalism). This technology is currently being deployed in the Consolidated Edison grid in New York, and a 3 mile long cable system is planned for installation in Commonwealth Edison's Chicago grid [106].

5.6.3 *Rotating Machines*

Another potentially large market for 2G HTS wire is in rotating machines, such as motors and generators. Typically these HTS machines are designed with HTS rotor field coils, which operate with dc currents, while the stator coils, which experience high ac currents, are made of copper. A major advantage of these HTS-based machines is that they can generate a very high torque in a compact size, allowing the design of high efficiency, light-weight, compact machines.

The first large-scale demonstration of such a HTS-based machine was a 36.5 MW HTS ship propulsion motor (based on 1G HTS wire) produced by AMSC and Northrop-Grumman, in 2009, for the US Navy, which has a long-term goal of converting to an all-electric fleet. The motor, which is less than half the size of a conventional motor, would reduce a ship's weight by over 200 metric tons. Such compact, efficient electric propulsion systems will enable flexibility in ship design and more efficient integration of a ship's energy-usage. This will allow an increase in the cargo or passenger space or, in the case of the military, additional or more powerful weapon systems. Additionally, the elimination of rotor losses leads to higher efficiency, especially under partial-load conditions, resulting to longer cruising ranges and greater fuel economy.

The need for clean, carbon-free renewable energy has fueled rapid growth of wind power and large off-shore wind farms. The economics of off-shore wind farm

installations favor wind turbines with the highest possible power ratings. However, higher power ratings increase the size and weight of conventional turbines, making installation more difficult and costly. Thus there is a growing interest in the development of HTS-based generators that can be used in off-shore wind turbines rated at 10 MW and greater. The first demonstration of a full-scale HTS-based wind turbine is a number of years off, with current activities focused on testing of sub-scale designs, verification of the cryogenic cooling systems and most importantly reducing the total wire cost through improvements in performance to reduce the amount of wire needed and through reduction in manufacturing costs.

5.6.4 Other Applications

2G HTS wire is also being developed for a variety of defense applications including power and degaussing cables, motors and generators. Although these applications do not represent a large market, they are performance rather than cost driven and will likely be among the first uses of 2G HTS wire. Other applications, which AMSC considers longer-term or niche markets, include medical or industrial MRI's and NMR's, high field research magnets, magnetic levitation, transformers, superconducting magnetic energy storage (SMES), fusion, directed energy weapons and current leads.

5.7 Summary

The discovery of the HTS materials in the late 1980s provided the foundation for today's superconductor wire technology. This initial discovery rapidly led to the basic research focused on understanding the vortex physics that controls the critical current density of the HTS materials, and the complex chemistry and material science of the (RE)BCO film growth. This basic science research slowly evolved into the applied research and development directed at innovative manufacturing technologies; the development of high-performance, robust, long length conductors; the development of concepts for the use of these new HTS materials and finally the design for HTS-based electric power equipment. Now after nearly three decades of research and development, the HTS wire technology has achieved the maturity level where it can start to be deployed in the "real-world" applications. As the commercialization of this revolutionary technology progresses we may finally see the broad impact envisioned at the time of its discovery.

The successful development of this technology at AMSC required assembling a diverse team of scientists and engineers who thought "out-of-the-box" and were not confined by conventional thinking. The ASMC team was built around key people with backgrounds in chemistry, physics, material science, mathematics, ceramics,

geology, computer modeling, mechanical and electrical engineering. This combination of scientists and engineers was able to address the fundamental science of the materials, develop innovative manufacturing processes and equipment and identify applications and develop product specifications. The successful development of such challenging technologies requires contributors who are experts in specific scientific or engineer disciplines, but can also effectively work in related fields.

References

1. M.W. Rupich, E.E. Hellstrom, Bi-Ca-Sr-Cu-O HTS Wire, in *100 Years of Superconductivity*, eds. by H. Rogalla, P.H. Kes (CRC Press, Boca Raton, 2012), Chap. 11.4
2. <http://ir.amsc.com/releasedetail.cfm?ReleaseID=725019>
3. <http://ir.amsc.com/releasedetail.cfm?ReleaseID=736299>
4. S.H. Sohn, J.H. Lim, B.M. Yang, S.K. Lee, H.M. Jang, Y.H. Kim, H.S. Yang, D.L. Kim, H. R. Kim, Y.J. Won, S.D. Hwang, Design and development of 500 m long HTS cable system in the KEPCO power grid, Korea. *Physica C: Superconduct.* **470**, 1567 (2010)
5. C. Ryu, H. Jang, C. Choi, Y. Kim, H. Kim, Current status of demonstration and commercialization of HTS cable system in grid in Korea, in *Proceedings of 2013 IEEE International Conference on Applied Superconductivity and Electromagnetic Devices*, Beijing, China, 25–27 Oct 2013, ID3231, p. 539
6. http://www.lscns.com/pr/news_read.asp?idx=2953&pageno=1&kType=&kWord
7. S. Jin, R.C. Sherwood, R.B. van Dover, T.H. Tiefel, D.W. Johnson Jr, High T_c superconductors-composite wire fabrication. *Appl. Phys. Lett.* **51**, 203 (1987)
8. Superconductivity: Is the Party Over? *Science*, **244**, 914 (1989)
9. <http://www.nytimes.com/1989/06/06/us/superconductors-showing-a-flaw-that-dims-hope.html>
10. T. Hikata, K. Sato, H. Hitotsuyanagi, Ag-sheathed Bi-Pb-Sr-Ca-Cu-O superconducting wires with high critical current density. *Jpn. J. Appl. Phys.* **L28**, 82 (1989)
11. L.N. Bulaevskii, J.R. Clem, L.I. Glazman, A.P. Malozemoff, Model for the low-temperature transport of Bi-based high-temperature superconducting tapes. *Phys. Rev. B* **45**, 2545 (1992)
12. L.N. Bulaevskii, L.L. Daemen, M.P. Maley, J.Y. Coulter, Limits to the critical current in high- T_c superconducting tapes. *Phys. Rev. B* **48**, 13798 (1993)
13. K. Sato, Bismuth-based oxide (BSCCO) high-temperature superconducting wires for power grid applications: properties and fabrication, in *Superconductors in the Power Grid*, ed. by C. Rey (Elsevier, Amsterdam, 2015), Chap. 3
14. S.L. Cooper, K.E. Gray, in *Physical Properties of High Temperature Superconductors*, ed. by D.M. Ginsberg (World Scientific, Singapore, 1994), vol. IV, p. 61
15. Y. Jia, U. Welp, G.W. Crabtree, W.K. Kwok, A.P. Malozemoff, M.W. Rupich, S. Fleshler, J.R. Clem, Microstructure dependence of the c-axis critical current density in second-generation YBCO tapes. *J. Appl. Phys.* **110**(8), 083923 (2011)
16. M. Tinkham, *Introduction to Superconductivity*, 2nd edn. (McGraw-Hill, New York, 1996)
17. D. Dimos, P. Chaudhari, J. Mannhart, Superconducting transport properties of grain boundaries in $\text{YBa}_2\text{Cu}_3\text{O}_7$ bicrystals. *Phys. Rev. B* **41**, 4038 (1990)
18. H. Hilgenkamp, J. Mannhart, Grain boundaries in high- T_c superconductors. *Rev. Mod. Phys.* **74**, 485 (2002)
19. Y. Iijima, N. Tanabe, Y. Ikeno, O. Kohno, Biaxially aligned $\text{YBa}_2\text{Cu}_3\text{O}_{7-x}$ thin film tapes. *Physica C: Superconduct.* **185**, 1959 (1991)
20. Y. Iijima, N. Tanabe, O. Kohno, Y. Ikeno, In-plane aligned $\text{YBa}_2\text{Cu}_3\text{O}_{7-x}$ thin films deposited on polycrystalline metallic substrates. *Appl. Phys. Lett.* **60**, 769 (1992)

21. Y. Iijima, K. Kakimoto, M. Kimura, K. Takeda, T. Saitoh, Reel to reel continuous formation of Y-123 coated conductors by IBAD and PLD method. *IEEE Trans. Appl. Superconduct.* **11**, 2816 (2001)
22. M.W. Rupich, Second-generation (2G) coated high-temperature superconducting cables and wires for power grid applications, in *Superconductors in the Power Grid*, ed. by C. Rey (Elsevier, Amsterdam, 2015), Chap. 4
23. D.P. Norton, A. Goyal, J.D. Budai, D.K. Christen, D.M. Kroeger, E.D. Specht, Q. He, B. Saffian, M. Paranthaman, C.E. Klabunde, D.F. Lee, B.C. Sales, F.A. List, Epitaxial $\text{YBa}_2\text{Cu}_3\text{O}_7$ on biaxially textured nickel (001): an approach to superconducting tapes with high critical current density. *Science* **274**, 755 (1996)
24. E.D. Specht, A. Goyal, D.F. Lee, F.A. List, D.M. Kroeger, M. Paranthaman, R.K. Williams, D.K. Christen, Cube-textured nickel substrates for high-temperature superconductors. *Superconduct. Sci. Technol.* **11**, 945 (1998)
25. M.P. Goyal, U. Schoop, The RABiTS approach: using rolling-assisted biaxially textured substrates for high-performance YBCO superconductors. *MRS Bull.* **29**, 552 (2004)
26. P.N. Ardent, S.R. Foltyn, Biaxially textured IBAD-MgO templates for YBCO-coated conductors. *MRS Bull.* **29**, 543 (2004)
27. Y. Iijima, K. Kakimoto, Y. Yamada, T. Izumi, T. Saitoh, Y. Shiohara, Research and development of biaxially textured IBAD-GZO templates for coated superconductors. *MRS Bull.* **29**, 564 (2004)
28. T. Kato, Y. Iijima, T. Muroga, T. Saitoh, T. Hirayama, I. Hirabayashi, Y. Yamada, T. Izumi, Y. Shiohara, Y. Ikuhara, TEM observations of $\text{Gd}_2\text{Zr}_2\text{O}_7$ films formed by the ion-beam-assisted deposition method on an Ni-based alloy. *Physica C: Superconduct.* **392–396**, 790 (2003)
29. C.P. Wang, K.B. Do, M.R. Beasley, T.H. Geballe, R.H. Hammond, Deposition of in-plane textured MgO on amorphous Si_3N_4 substrates by ion-beam-assisted deposition and comparisons with ion-beam-assisted deposited yttria-stabilized-zirconia. *Appl. Phys. Lett.* **71**, 2955 (1997)
30. X. Xiong, S. Kim, K. Zdun, S. Sambandam, A. Rar, K.P. Lenseth, V. Selvamanickam, Progress in high throughput processing of long-length, high quality, and low cost IBAD MgO buffer tapes at SuperPower. *IEEE Trans. Appl. Superconduct.* **19**, 3319 (2009)
31. K.P. Ko, H.S. Ha, H.K. Kim, K.K. Yu, R.K. Ko, S.H. Moon, S.S. Oh, C. Park, S.I. Yoo, Fabrication of highly textured IBAD-MgO template by continuous reel-to-reel process and its characterization. *Physica C: Superconduct.* **463–465**, 564 (2007)
32. S. Hanyu, C. Tashita, T. Hayashida, Y. Hanada, K. Morita, Y. Sutoh, N. Nakamura, H. Kutami, M. Igarashi, K. Kakimoto, Y. Iijima, T. Saitoh, Long-length IBAD-MgO buffer layers for high performance RE-123 coated conductors by a large ion beam source. *Physica C: Superconduct.* **470**, 1227 (2010)
33. M. Paranthaman, T. Aytug, D.K. Christen, P.N. Arendt, S.R. Foltyn, J.R. Groves, L. Stan, R. F. DePaula, H. Wang, T.G. Holesinger, Growth of thick $\text{YBa}_2\text{Cu}_3\text{O}_{7-\delta}$ films carrying a critical current of over 230 A/cm on single LaMnO_3 -buffered ion-beam assisted deposition MgO substrates. *J. Mater. Res.* **18**, 2055 (2003)
34. K. Hasegawa, K. Fujino, H. Mukai, M. Konishi, K. Hayashi, K. Sato, S. Honjo, Y. Sato, H. Ishii, Y. Iwata, Biaxially aligned YBCO film tapes fabricated by all pulsed laser deposition. *Appl. Superconduct.* **4**, 487 (1996)
35. M. Dürschnabel, Z. Aabdin, V. Große, M. Bauer, G. Sigl, W. Prusseit, O. Eibl, Growth of biaxially-textured MgO buffer layers by inclined substrate deposition. *Phys. Procedia* **36**, 1546 (2012)
36. M. Bauer, R. Metzger, R. Semerad, P. Berberich, H. Kinder, Inclined substrate deposition by evaporation of magnesium oxide for coated conductors. *MRS Proc.* **585**, 35 (1999)
37. N.M. Strickland, N.J. Long, E.F. Talantsev, P. Hoefakker, J.A. Xia, M.W. Rupich, W. Zhang, X. Li, T. Kodenkandath, Y. Huang, Nanoparticle additions for enhanced flux pinning in YBCO HTS films. *Current Appl. Phys.* **8**, 372 (2008)

38. Y. Chen, V. Selvamanickam, Y. Zhang, Y. Zuev, C. Cantoni, E. Specht, M.P. Paranthaman, T. Aytug, A. Goyal, D. Lee, Enhanced flux pinning by BaZrO₃ and (Gd,Y)₂O₃ nanostructures in metal organic chemical vapor deposited GdYBCO high temperature superconductor tapes. *Appl. Phys. Lett.* **94**, 062513 (2009)
39. R.J. Gupta, E.I. Cooper, E.A. Giess, J.I. Landman, B.W. Hussey, Superconducting oxide films with high transition temperature prepared from metal trifluoroacetate precursors. *Appl. Phys. Lett.* **52**, 2077 (1988)
40. P.C. McIntyre, M.J. Cima, M.F. Ng, Metalorganic deposition of high-Jc Ba₂YCu₃O_{7-x} thin films from trifluoroacetate precursors onto (100) SrTiO₃. *J. Appl. Phys.* **68**, 4183 (1990)
41. M.W. Rupich, D.T. Verebelyi, W. Zhang, T. Kodenkandath, X. Li, Metalorganic deposition of YBCO films for second-generation high-temperature superconductor wires. *MRS Bull.* **29**, 572 (2004)
42. P.C. McIntyre, M.J. Cima, Heteroepitaxial growth of chemically derived *ex situ* Ba₂YCu₃O_{7-x} thin films. *J. Mater. Res.* **9**, 2219 (1994)
43. M. Yoshizumi, T. Nakanishi, J. Matsuda, K. Nakaoka, Y. Sutoh, T. Izumi, Y. Shiohara, Crystal growth of YBCO coated conductors by TFA-MOD method. *Physica C: Superconduct.* **468**, 1531 (2008)
44. X. Obradors, T. Puig, S. Ricart, M. Coll, J. Gazquez, A. Palau, X. Granados, Growth, nanostructure and vortex pinning in superconducting YBa₂Cu₃O₇ thin films based on trifluoroacetate solutions. *Superconduct. Sci. Technol.* **25**, 123001 (2012)
45. D. Dijkkamp, T. Venkatesan, X.D. Wu, S.A. Shaheen, N. Jisrawi, Y.H. Min-Lee, W.L. McLean, M. Croft, Preparation of Y-Ba-Cu oxide superconductor thin films using pulsed laser evaporation from high Tc bulk material. *Appl. Phys. Lett.* **51**, 619 (1987)
46. S.R. Foltyn, H. Wang, L. Civale, Q.X. Jia, P.N. Arendt, B. Maiorov, Y. Li, M.P. Maley, J.L. MacManus-Driscoll, Overcoming the barrier to 1000 A/cm width superconducting coatings. *Appl. Phys. Lett.* **87**, 162505 (2005)
47. H.M. Manasevit, Single-crystal Gallium Arsenide on insulating substrates. *Appl. Phys. Lett.* **12**, 156 (1968)
48. V. Selvamanickam, G. Carota, M. Funk, N. Vo, P. Haldar, U. Balachandran, M. Chudzik, P. Arendt, J.R. Groves, R. DePaula, B. Newnam, High-current Y-Ba-Cu-O coated conductor using metal organic chemical-vapor deposition and ion-beam-assisted deposition. *IEEE Trans. Appl. Superconduct.* **19**, 3379 (2001)
49. P. Berberich, B. Utz, W. Prusseit, H. Kinder, Homogeneous high quality YBa₂Cu₃O₇ films on 3" and 4" substrates. *Physica C: Superconduct.* **219**, 497 (1994)
50. S.S. Oh, H.S. Ha, H.S. Kim, R.K. Ko, K.J. Song, D.W. Ha, T.H. Kim, N.J. Lee, D. Youm, J. S. Yang, H.K. Kim, K.K. Yu, S.H. Moon, K.P. Ko, S.I. Yoo, Development of long-length SmBCO coated conductors using a batch-type reactive co-evaporation method. *Superconduct. Sci. Technol.* **21**, 034003 (2008)
51. T. Ohnishi, J.-U. Huh, R.H. Hammond, W. Jo, High rate in situ YBa₂Cu₃O₇ film growth assisted by liquid phase. *J. Mater. Res.* **19**, 977 (2004)
52. J.L. MacManus-Driscoll, A. Kursumovic, B. Maiorov, L. Civale, Q.X. Jia, S.R. Foltyn, H. Wang, YBa₂Cu₃O₇ Coated conductor grown by hybrid liquid phase epitaxy. *IEEE Trans. Appl. Superconduct.* **17**, 2537 (2007)
53. S.H. Moon, Recent progress of 2G superconducting wire at SuNAM. Presentation at the International Workshop on coated Conductors for Applications 2014, Jeju, Korea, 2 Dec 2014
54. M.W. Rupich, X. Li, S. Sathyamurthy, C.L.H. Thieme, K. DeMoranville, J. Gannon, S. Fleshler, Second generation wire development at AMSC. *IEEE Trans. Appl. Superconduct.* **23**, 6601205 (2013)
55. X. Li, M.W. Rupich, C.L.H. Thieme, M. Teplitsky, D. Buczek, E. Siegal, D. Tucker, J. Schreiber, K. DeMoranville, J. Inch, R. Savoy, S. Fleshler, The development of second generation HTS wire at American superconductor. *IEEE Trans. Appl. Superconduct.* **19**, 3231 (2009)

56. J.B. Goyal, D.M. Kroeger, D. Norton, E.D. Specht, D.K. Christen, Preparing biaxially textured metal alloy article; superconductors, United States Patent No. 5,741,377 (1998)
57. V. Goler, G. Sachs, Walz und Rekristallizationstextur regular-flachenzentrierter Metalle III, IV. Z. Angew. Phys. **59**, 477 (1929)
58. P.C.J. Gallagher, The influence of alloying, temperature and related effects on the stacking fault energy. Met. Trans. **1**, 2429 (1970)
59. S.L. Shang, C.L. Zacherl, H.Z. Fang, Y. Wang, Y. Du, Z.K. Liu, Effects of alloying element and temperature on the stacking fault energies of dilute Ni-base superalloys. J. Phys: Condens. Matter **24**, 505403 (2012)
60. R.M. Bozorth, *Ferromagnetism* (D. van Nostrand, New York, 1951)
61. R. Huhne, J. Eickemeyer, V.S. Sarma, A. Guth, T. Thersleff, J. Freudenberger, O. de Haas, M. Weigand, J.H. Durrell, L. Schultz, B. Holzapfel, Application of textured highly alloyed Ni–W tapes for preparing coated conductor architectures. Superconduct. Sci. Technol. **23**, 034015 (2010)
62. L. Delannay, Observation and modelling of grain interactions and grain subdivision in rolled cubic polycrystals. Ph.D. Thesis, Catholic University, Leuven, May 2001
63. F.J. Humphreys, M. Hatherley, *Recrystallization and Related Annealing Phenomena*, 2nd edn. (Elsevier, Oxford, 2004), Chap. 12
64. D.M. Feldmann, T.G. Holesinger, R. Feenstra, C. Cantoni, W. Zhang, X. Li, M. Rupich, A. Malozemoff, A. Gurevich, D.C. Larbalestier, Grain orientations and grain boundary networks of $\text{YBa}_2\text{Cu}_3\text{O}_{7-\delta}$ films deposited by metalorganic and pulsed laser deposition on biaxially textured Ni–W substrates. J. Mater. Res. **21**, 923 (2006)
65. J.M.S. Skakle, Crystal chemical substitutions and doping of $\text{Yba}_2\text{Cu}_3\text{O}_x$ and related superconductors. Mater. Sci. Eng. **R23**, 1 (1998)
66. G.D.P. Norton, J.D. Budai, M. Paranthaman, E.D. Specht, D.M. Kroeger, D.K. Christen, Q. He, B. Saffian, F.A. List, D.F. Lee, P.M. Martin, C.E. Klabunde, E. Hartfield, V.K. Sikka, High critical current density superconducting tapes by epitaxial deposition of $\text{YBa}_2\text{Cu}_3\text{O}_x$ thick films on biaxially textured metals. Appl. Phys. Lett. **69**, 1795 (1996)
67. Q. He, D.K. Christen, J.D. Budai, E.D. Specht, D.F. Lee, A. Goyal, D.P. Norton, M. Paranthaman, F.A. List, D.M. Kroeger, Deposition of biaxially-oriented metal and oxide buffer-layer films on textured Ni tapes: new substrates for high-current, high-temperature superconductors. Physica C: Superconduct. **275**, 155 (1997)
68. M. Paranthaman, D.F. Lee, A. Goyal, E.D. Specht, P.M. Martin, X. Cui, J.E. Mathis, R. Feenstra, D.K. Christen, D.M. Kroeger, Growth of biaxially textured RE_2O_3 buffer layers on rolled-Ni substrates using reactive evaporation for HTS-coated conductors. Superconduct. Sci. Tech. **12**, 319 (1999)
69. M.N. Molodyk, S. Street, L. Castellani, A. Ignatiev, All-MOCVD technology for coated conductor fabrication. IEEE Trans. Appl. Superconduct. **21**, 3175 (2011)
70. F.A. List, A. Goyal, M. Paranthaman, D.P. Norton, E.D. Specht, D.F. Lee, D.M. Kroeger, High J_c YBCO films on biaxially textured Ni with oxide buffer layers deposited using electron beam evaporation and sputtering. Physica C: Superconduct. **302**, 87 (1998)
71. D.P. Norton, A. Goyal, J.D. Budai, D.K. Christen, D.M. Kroeger, E.D. Specht, Q. He, B. Saffian, M. Paranthaman, C.E. Klabunde, D.F. Lee, B.C. Sales, F.A. List, Epitaxial $\text{YBa}_2\text{Cu}_3\text{O}_7$ on biaxially textured nickel (001): an approach to superconducting tapes with high critical current density. Science **274**, 755 (1996)
72. T. Aytug, M. Paranthaman, B.W. Kang, S. Sathyamurthy, A. Goyal, D.K. Christen, $\text{La}_0.7\text{Sr}_0.3\text{MnO}_3$: A single, conductive-oxide buffer layer for the development of $\text{YBa}_2\text{Cu}_3\text{O}_{7-\delta}$ coated conductors. Appl. Phys. Lett. **79**, 2205 (2001)
73. T. Aytug, J.Z. Wu, C. Cantoni, D.T. Verebelyi, E.D. Specht, M. Paranthaman, D.P. Norton, D.K. Christen, R.E. Ericson, C.L. Thomas, Growth and superconducting properties of $\text{YBa}_2\text{Cu}_3\text{O}_{7-\delta}$ films on conductive SrRuO_3 and LaNiO_3 multilayers for coated conductor applications. Appl. Phys. Lett. **76**, 760 (2000)
74. S. Sathyamurthy, M. Paranthaman, H.Y. Zhai, S. Kang, T. Aytug, C. Cantoni, K.J. Leonard, E.A. Payzant, H.M. Christen, A. Goyal, X. Li, U. Schoop, T. Kodenkandath, M.W. Rupich,

- Chemical solution deposition of lanthanum zirconate barrier layers applied to low-cost coated-conductor fabrication. *J. Mater. Res.* **19**, 2117 (2004)
75. K. Knoth, R. Hühne, S. Oswald, L. Schultz, B. Holzapfel, Highly textured $\text{La}_2\text{Zr}_2\text{O}_7$ buffer layers for YBCO-coated conductors prepared by chemical solution deposition. *Superconduct. Sci. Tech.* **18**, 334 (2005)
 76. C. Cantoni, D.K. Christen, R. Feenstra, A. Goyal, G.W. Ownby, D.M. Zehner, D.P. Norton, Reflection high-energy electron diffraction studies of epitaxial oxide seed-layer growth on rolling-assisted biaxially textured substrate Ni(001): The role of surface structure and chemistry. *Appl. Phys. Lett.* **79**, 3077 (2001)
 77. C. Cantoni, D.K. Christen, D.K. Heatherly, M.M. Kowalewski, F.A. List, A. Goyal, G. Ownby, D.M. Zehner, B.W. Kang, D.M. Kroeger, Quantification and control of the sulfur c (2×2) superstructure on $\{100\}\{100\}$ Ni for optimization of YSZ, CeO_2 and SrTiO_3 seed layers texture. *J. Mat. Res.* **17**, 2549 (2002)
 78. C. Cantoni, D.K. Christen, A. Goyal, L. Heatherly, F.A. List, G.W. Ownby, D.M. Zehner, H. M. Christen, C.M. Rouleau, Growth of oxide seed layers on Ni and other technologically interesting metal substrates: issues related to formation and control of sulfur superstructures for texture optimization. *IEEE Trans. Appl. Superconduct.* **13**, 2646 (2003)
 79. Y. Tokunaga, T. Honjo, T. Izumi, Y. Shiohara, Y. Iijima, T. Saitoh, T. Goto, A. Yoshinaka, A. Yajima, Advanced TFA-MOD process of high critical current YBCO films for coated conductors. *Cryogenics* **44**, 817 (2004)
 80. H. Fuji, R. Teranishi, Y. Kito, J. Matsuda, K. Nakaoka, T. Izum, Y. Shiohara, Y. Yamada, A. Yajima, T. Saitoh, Progress on TFA-MOD coated conductor development. *Physica C: Superconduct.* **426–431**, 938 (2005)
 81. K. Tada, J. Yoshida, N. Mori, K. Yamada, R. Teranishi, M. Mukaida, T. Kiss, M. Inoue, Y. Shiohara, T. Izumi, J. Matsuda, K. Nakaoka, Growth process of Ba-poor YBCO film fabricated by TFA-MOD process. *Physica C: Superconduct.* **468**, 1554 (2008)
 82. J. Yoshida, K. Tada, T. Tanaka, N. Mori, K. Yamada, R. Teranishi, M. Mukaida, T. Kiss, M. Inoue, Y. Shiohara, T. Izumi, K. Nakaoka, J. Matsuda, Effect of calcination conditions on microstructures and J_c of YBCO films fabricated by TFA-MOD method. *Physica C: Superconduct.* **468**, 1550 (2008)
 83. C.S. Li, Y.F. Lu, P.X. Zhang, Z.M. Yu, B.W. Tao, J.Q. Feng, L.H. Jin, Study of modified TFA-MOD method for YBCO film growth. *Physics Procedia* **36**, 1620 (2012)
 84. M.W. Rupich, X. Li, S. Sathyamurthy, C.L.H. Thieme, K. DeMoranville, J. Gannon, S. Fleshler, Second generation wire development at AMSC. *IEEE Trans. Appl. Superconduct.* **23**, 6601205 (2013)
 85. M.W. Rupich, X. Li, S. Sathyamurthy, C. Thieme, S. Fleshler, Advanced development of TFA-MOD coated conductors. *Physica C: Superconduct.* **471**, 919 (2011)
 86. D.W. Hazelton, Advances in 2G HTS conductor for high field applications, presented at the *Low Temperature High Field Superconductivity Workshop*, St. Petersburg, FL Nov. 5, 2013: http://www.superpower-inc.com/system/files/2013_1105+LTHFSW+SuperPower+FINAL.pdf
 87. W. Schmidt, H.-P. Kraemer, N.-W. Neumueller, U. Schoop, D. Verebelyi, A.P. Malozemoff, Investigation of YBCO coated conductors for fault current limiter applications. *IEEE Trans. Appl. Superconduct.* **17**, 3471 (2007)
 88. V. Selvamanickam, Y. Yao, Y. Chen, T. Shi, Y. Liu, N.D. Khatri, J. Liu, C. Lei, E. Galstyan, G. Majkic, The low-temperature, high-magnetic-field critical current characteristics of Zr-added (Gd, Y)Ba₂Cu₃O_x superconducting tapes. *Superconduct. Sci. Tech.* **25**, 125013 (2012)
 89. Y. Jia, M. LeRoux, D.J. Miller, J.G. Wen, W.K. Kwok, U. Welp, M.W. Rupich, X. Li, S. Sathyamurthy, S. Fleshler, A.P. Malozemoff, A. Kayani, O. Ayala-Valenzuela, L. Civale, Doubling the critical current density of high temperature superconducting coated conductors through proton irradiation. *Appl. Phys. Lett.* **103**, 122601 (2013)
 90. M. W. Rupich, S. Sathyamurthy, S. Fleshler, Q. Li, V. Solovyov, T. Ozaki, U. Welp, W. K. Kwok, M. Leroux, A. E. K., D. J. Miller, K. Kihlstrom, L. Civale, S. Eley, A. Kayani,

- Engineered Pinning Landscapes for Enhanced 2G Coil Wire. *IEEE Trans. on App Supercond.* (in press)
91. L. Heatherly, H. Hsu, S.H. Wee, J. Li, S. Sathyamurthy, M. Paranthaman, A. Goyal, Slot die coating and conversion of LZO on rolling assisted biaxially textured Ni-W substrates with and without a very thin seed layer in low vacuum. *IEEE Trans. Appl. Superconduct.* **17**, 3417 (2007)
 92. M.S. Bhuiyan, M. Paranthaman, S. Sathyamurthy, Chemical solution-based epitaxial oxide films on biaxially textured Ni-W substrates with improved out-of-plane texture for YBCO-coated conductors. *J. Electron. Mater.* **36**, 1270 (2007)
 93. N.-W. Neumueller, W. Schmidt, H.-P. Kraemer, A. Otto, J. Maguire, J. Yuan, D. Folts, W. Romanosky, B. Gamble, D. Madura, A.P. Malozemoff, N. Lallouet, S.P. Ashworth, J.O. Willis, S. Ahmed, Development of resistive fault current limiters based on YBCO coated conductors. *IEEE Trans. Appl. Superconduct.* **19**, 1950 (2009)
 94. J.B. Na, D.K. Park, S.E. Yang, Y.J. Kim, K.S. Chang, H. Kang, T.K. Ko, Experimental verification of non-inductive wound solenoid coil for large transport currents. *Physica C: Superconduct.* **469**, 1754 (2009)
 95. T. Yazawa, K. Koyanagi, M. Takahashi, K. Toba, H. Takigami, M. Urata, Y. Iijima, T. Saitoh, N. Amemiya, Y. Shiohara, T. Ito, Development of 6.6 kV/600 A superconducting fault current limiter using coated conductors. *Physica C: Superconduct.* **469**, 1740 (2009)
 96. P. Tixador, N.T. Nguyen, Design of ReBaCuO-coated conductors for FCL. *Superconduct. Sci. Technol.* **25**, 014009 (2012)
 97. http://www.amsc.com/library/SAFCL_BRO_0812.pdf
 98. H. Yumura, Y. Ashibe, H. Itoh, M. Ohya, M. Watanabe, T. Masuda, C.S. Weber, Phase II of the Albany HTS cable project. *IEEE Trans. Appl. Superconduct.* **19**, 1698 (2009)
 99. Super3C Project news release, 17 March 2009. <http://www.brucker-est.com/super3c.html>
 100. M. Ohya, Y. Ashibe, M. Watanabe, T. Minamino, H. Yumura, T. Masuda, T. Kato, Development of RE-123 superconducting cable. *IEEE Trans. Appl. Superconduct.* **19**, 1766 (2009)
 101. S. Mukoyama, M. Yagi, T. Masuda, N. Amemiya, A. Ishiyama, N. Kashima, S. Nagaya, Y. Aoki, M. Yoshizumi, Y. Yamada, T. Izumi, Y. Shiohara, Development of (RE)BCO cables for HTS power transmission lines. *Physica C: Superconduct.* **469**, 1688 (2009)
 102. J.F. Maguire, F. Schmidt, S. Bratt, T.E. Welsh, J. Yuan, Installation and testing results of Long Island transmission level HTS cable. *IEEE Trans. Appl. Superconduct.* **19**, 1692 (2009)
 103. J. Maguire, D. Folts, J. Yuan, D. Lindsay, D. Knoll, S. Bratt, Z. Wolff, S. Kurtz, Development and demonstration of a fault current limiting HTS cable to be installed in the Con Edison grid. *IEEE Trans. Appl. Superconduct.* **19**, 1740 (2009)
 104. C.M. Rey, R.C. Duckworth, J.A. Demko, A. Ellis, D.R. James, M.J. Gouge, E. Tuncer, Test results for a 25 meter prototype fault current limiting HTS cable for project Hydra. *AIP Conf. Proc.* **1218**, 453 (2010)
 105. J. Maguire, D. Folts, J. Yuan, N. Henderson, D. Lindsay, D. Knoll, C. Rey, R. Duckworth, M. Gouge, Z. Wolff, S. Kurtz, Status and progress of a fault current limiting HTS cable to be installed in the Con Edison grid. *AIP Conf. Proc.* **1218**, 445 (2010)
 106. <http://ir.amsc.com/releasedetail.cfm?ReleaseID=860164>